A retrieval of the drop size distribution from microwave link signal fluctuations

Author:
Emily Seager

Supervisors:
dr. Hidde Leijnse[1]
prof. dr. ir. Jason Frank[2]
[1]Royal Netherlands Meteorological Institute
[2]Mathematical Institute, Utrecht University

Master's Thesis
in
Mathematical Sciences

Written in combination with an internship at the Royal Netherlands Meteorological Institute

November 2018

Contents

1 Introduction

Accurate rainfall measurements are crucial for weather forecasting models, water resource management and flood prediction. The most common and well used measure of rain is the rainfall intensity, i.e. the amount of rain per unit of time.

It is true that reliable estimates of rainfall intensity can be obtained through instruments such as rain gauges, provided they are well maintained; however, they only provide point measurements. Another setback for this method is that in many parts of the world, particularly in developing countries, there is a real scarcity of such equipment. Recent research [1] has looked at the potential of using microwave signals from cellular communication networks for rainfall measurements. A motivation for such methods is how ubiquitous these networks have become in the last decade, with the huge demand on mobile phone usage. In 2016, an estimated 63 per cent of the global population owned a mobile phone, with that figure expected to rise another 3 per cent by next year [2]. The idea in a communication network is that a beam composing of microwaves travels from a transmitter to a receiver. This structure is known as a microwave link. This research has analysed the attenuation of these link signals due to rainfall. This is possible because the power loss along links is recorded by the mobile phone company to monitor their network stability.

Attenuation methods give very encouraging results; however, the results often over exaggerate the rainfall intensity. The main reason for this is believed to be due to a wet film that appears on the antenna due to rainfall. Another issue associated with these methods is that it can be hard to properly determine the signal level during dry weather due to fluctuations caused by atmospheric turbulence. In this study we introduce a method that could be insensitive to such problems.

Instead of looking at the reduction in power of a signal we propose to analyse the fluctuations to microwave link signals, using the idea that when a wave travels through a rain drop it will cause a slight perturbation to the wavefront. There is huge potential to gain more accurate precipitation measurements through studying fluctuations rather than signal attenuation because base-line fluctuations predominately occur at lower frequencies, whereas fluctuations from rainfall occur at a wider range. Moreover, a high frequency signal is much less likely to be sensitive to the wetting of the antenna. Using fluctuation analysis methods we hope for a retrieval of the drop size distribution, which can give detailed characteristics of precipitation.

There is limited research into amplitude fluctuations of electromagnetic waves caused by rainfall. The only work that is known currently on this topic is the analysis of a laser beam propagating through rain [3]. This laser beam is taken to be a plane wave, and the wavelength $\sim 10^{-7}$m, the very high end of the electromagnetic spectrum. Studying the effects of rain on microwaves will be quite different. Microwaves are similar to light in that they are also electromagnetic waves; however, they have a wavelength in the much lower regions of the spectrum. In general the wavelength is $\sim 10^{-3}$m. This wavelength has a similar order of magnitude to the size of a rain drop, compared with that of a laser beam and so the result will be quite different. The geometry of the problem will also differ from that of previous work because we are not assuming plane waves. The beam of the microwave signal leaves the transmitter, and the wave propagates in all directions, as concentric spheres. This is known as a spherical wave and this property will be taken into consideration in this study.

We begin with an introduction into scattering theory of electromagnetic waves, which is applicable to rainfall. From this we can obtain an expression for the amplitude fluctuations caused by a monodisperse distribution of raindrops. We then determine certain statistical properties of these fluctuations, such as the temporal covariance function. From here we can extend by assuming a more realistic distribution of raindrops and use statistical inference methods to try and retrieve the drop size distribution. As rainfall intensity is the most commonly used measure of rainfall, we will show how rainfall intensity can be obtained from the drop size distribution. We test our theoretical methods using data obtained from the Chilbolton Observatory. The data used does not come from a microwave link currently in use in a cellular communication network; however, it has very similar characteristics to those used in real networks. Testing our methods on real microwave link data can give us a good idea of the feasibility of this method, which can hopefully be a ket step in using mobile phone communications to give widespread rainfall estimates.

2 Formulation of the problem

In order to understand how waves propagate through rainfall we first need to illustrate some of the theory behind electromagnetic scattering. To begin, we will derive a time independent form of the wave equation. We then want to transform this random wave equation into a different expression which that can then be solved using a series expansion method, this is known as the Rytov approximation. This approximation provides a very useful technique in which one can solve the wave equation, when the amplitude variations are small. The idea behind this method is to express the total electric field as a product of the unperturbed field and another function to be determined, known as a surrogate function. In order for this method to work we note that we assume weak scattering.

An electric field is in general defined as a vector quantity, where the direction that this field takes at each point along its path defines the polarization of the field. We are assuming line-of-sight propagation, with very small angle scattering to be the most dominant, and so we can assume that the change in polarization in this case can be taken to be negligible. As a result of this we can take the electric field to be scalar, with E denoting a scalar field and $E : \mathbb{R}^3 \to \mathbb{R}$. We take the electric field to map to a real quantity because we are interested in the amplitude, which is the maximum electric field strength, and the real part of the electric field. We first state the well known scalar random-wave equation

$$\Delta E + k^2(1 + \varepsilon(\boldsymbol{r}))E = 0, \tag{2.1}$$

where ε describes the random dielectric variations of the medium, $\boldsymbol{r}$ is the position vector of the irregularity, and ΔE represents the Laplacian of E. We are considering a three dimensional coordinate space $\mathbb{R}^3$, with Cartesian coordinates (x, y, z), and $\boldsymbol{r} = (x, y, z)$. We also note that for this study we place the transmitter at the origin of coordinates. In order to carry out the series expansion approximation we can assume that a solution will be of the form

$$E(\boldsymbol{r}) = E_0(\boldsymbol{r}) \exp(\Psi(\boldsymbol{r})) \tag{2.2}$$

where $E_0(\boldsymbol{r})$ is the unperturbed electric field at position $\boldsymbol{r}$, and $\Psi(\boldsymbol{r})$ is a surrogate function to be discovered, which again we take to be a scalar quantity, with $\Psi : \mathbb{R}^3 \to \mathbb{C}$. Here the solution is chosen to be complex, so it will give us information about the amplitude and the phase of the wave. If we substitute (2.2) into (2.1), we arrive at the following

$$E_0\nabla^2 \exp(\Psi) + 2\nabla E_0 \cdot \nabla \exp(\Psi) + k^2\varepsilon E_0 \exp(\Psi) = -\exp\Psi\nabla^2 E_0 - k^2 E_0 \exp(\Psi). \tag{2.3}$$

We can see immediately that a factor of the unperturbed electric field E_0 can be dropped, where $\nabla E_0/E_0 = \nabla \ln E_0$ by the chain rule and using the second derivative of two scalar quantities $\nabla(fg) = f\nabla^2 g + 2\nabla f \cdot \nabla g + g\nabla^2 f$. Dividing through by $\exp(\Psi)$ gives

$$\nabla^2\Psi + |\nabla\Psi|^2 + 2\nabla \ln E_0 \cdot \nabla\Psi + k^2\varepsilon = 0, \tag{2.4}$$

where $\nabla^2 E_0 + k^2 E_0 = 0$ from the simple wave equation. It is reasonable to assume that the unperturbed field can be represented in a similar form to the function E we are trying to determine, and so

$$E_0(\boldsymbol{r}) = \exp(\psi_0(\boldsymbol{r})), \tag{2.5}$$

with ψ_0 being a dimensionless function, with the expression we will use in our series expansion solution being

$$\nabla^2\Psi + |\nabla\Psi|^2 + 2\nabla\psi_0 \cdot \nabla\Psi + k^2\varepsilon = 0. \tag{2.6}$$

To begin solving we will assume a solution of the form

$$\Psi(\boldsymbol{r}) = \psi_0(\boldsymbol{r}) + \varepsilon\psi_1(\boldsymbol{r}) + \varepsilon^2\psi_2(\boldsymbol{r}) + ... \tag{2.7}$$

Substituting (2.7) into (2.6), and equating equal powers of ε gives the following set of equations

$$\Delta\psi_0 + |\nabla\psi_0|^2 + k^2 = 0, \tag{2.8}$$

$$\Delta\psi_1 + 2\nabla\psi_0 \cdot \nabla\psi_1 + k^2\varepsilon = 0, \tag{2.9}$$

$$\Delta\psi_2 + 2\nabla\psi_0 \cdot \nabla\psi_2 + |\nabla\psi_1|^2 = 0. \tag{2.10}$$

$$\vdots \qquad\qquad \vdots$$

The Rytov solution is in general defined by the first order function $\psi_1(\boldsymbol{r})$, and so using (2.9) we substitute our following assumed solution

$$\psi_1(\boldsymbol{r}) = \Phi(\boldsymbol{r})\exp(-\psi_0(\boldsymbol{r})) \tag{2.11}$$

with $\Phi : \mathbb{R}^3 \to \mathbb{C}$ and $\psi_1 : \mathbb{R}^3 \to \mathbb{C}$. Using the identity $\Delta f = \nabla^2 f = (\nabla \cdot \nabla)f$ we give the gradient and Laplacian of ψ_1,

$$\nabla\psi_1 = -\nabla\psi_0 \exp^{-\psi_0} + \exp^{-\psi_0} \nabla\Phi \tag{2.12}$$

$$\nabla \cdot (\nabla\psi_1) = \Delta\psi_1 = -\Delta\psi_0\Phi e^{-\psi_0} - 2\nabla\psi_0 \cdot \nabla\Phi e^{-\psi_0} + |\nabla\psi_0|^2 + \Delta\Phi e^{-\psi_0} \tag{2.13}$$

Substituting (2.12) and (2.13)into (2.9) we have

$$\Delta\Phi - |\nabla\psi_0|^2\Phi - \Delta\psi_0\Phi = -e^{\psi_0}k^2\varepsilon. \tag{2.14}$$

Tatarskii [4] gives the solution of (2.14) as

$$\Phi(\boldsymbol{L}) = k^2 \int G(\boldsymbol{L}, \boldsymbol{r})\varepsilon(\boldsymbol{r})\exp(\psi(\boldsymbol{L}))d^3r, \tag{2.15}$$

where $G(\boldsymbol{L}, \boldsymbol{r})$ represents Green's function, with

$$G(\boldsymbol{L}, \boldsymbol{r}) = \frac{\exp(ik|\boldsymbol{L} - \boldsymbol{r}|)}{4\pi|\boldsymbol{L} - \boldsymbol{r}|}. \tag{2.16}$$

Here $\boldsymbol{L} \in \mathbb{R}^3$ represents the position of the receiver. Therefore

$$\psi_1(\boldsymbol{L}) = k^2 \int G(\boldsymbol{L}, \boldsymbol{r})\varepsilon(\boldsymbol{r})\exp(\psi(\boldsymbol{L}) - \psi(\boldsymbol{r}))d^3r, \tag{2.17}$$

which represents the solution at the receiver. Finally, substituting (2.5) back in we get

$$\psi_1(\boldsymbol{L}) = k^2 \int G(\boldsymbol{L}, \boldsymbol{r}) \varepsilon(\boldsymbol{r}) \frac{E_0(\boldsymbol{r})}{E_0(\boldsymbol{L})} d^3 r. \tag{2.18}$$

We are only considering single scattering in this study, i.e. we are assuming that a scattered wave front is only scattered by one irregularity and not scattered by any additional obstructions between the first scatterer and the receiver. Hence, equation (2.18) describes the single scattering term. The following relation links the amplitude and phase to the first order Rytov function,

$$\psi_1 = \chi + iP, \tag{2.19}$$

where χ represents the log-amplitude fluctuations and P represents the phase fluctuations. Taking the real part ψ_1 will give us the log-amplitude fluctuations. Here we are able to take the log amplitude as the experiment we will test our methods on is using a logarithmic receiver, as will be discussed in section (4.2). From equation (2.19), it can be easily seen that the amplitude fluctuations can be described by the real part of the above scattering integral, and so

$$\chi(\boldsymbol{L}) = \Re \left\{ k^2 \int G(\boldsymbol{L}, \boldsymbol{r}) \varepsilon(\boldsymbol{r}) \frac{E_0(\boldsymbol{r})}{E_0(\boldsymbol{L})} d^3 r \right\}. \tag{2.20}$$

2.1 Geometry describing spherical wave propagation

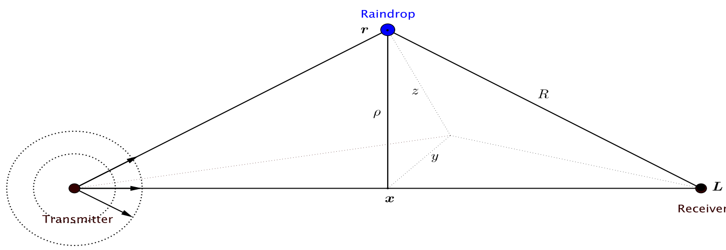

Figure 1: Here we show the geometry to describe the scattering of a spherical wave by a raindrop, where the receiver is at position $\boldsymbol{L}$, and $\boldsymbol{x}$ the horizontal position from the transmitter to the drop. Here $\rho = \sqrt{y^2 + z^2}$, and $x \gg p$. Also note that x,y and z are orthogonal to one another.

The geometry of Figure 1 is not to scale, as we expect the angle of scattering to be very small. We also assume our transmitter to act as a point source when emitting microwaves. This will simplify our model considerably. We can expand the square roots as follows

$$R = |\boldsymbol{L} - \boldsymbol{r}| = \sqrt{(L-x)^2 + \rho^2} \approx L - x + \frac{\rho^2}{2(L-x)} + ... \tag{2.21}$$

and

$$|\boldsymbol{r}| = \sqrt{x^2 + \rho^2} \approx x + \frac{\rho^2}{2x} + ... \tag{2.22}$$

If $E_0(\boldsymbol{r})$ is a spherical wave propagating from the origin, then

$$\frac{E_0(\boldsymbol{r})}{E_0(\boldsymbol{L})} = \frac{L}{\sqrt{x^2 + \rho^2}} \exp(ik(\sqrt{x^2 + \rho^2} - L)). \tag{2.23}$$

We have already stated that $\varepsilon(\boldsymbol{r})$ represents a small perturbation in the dielectric constant, caused by the presence of some turbulent eddy. We now make the assumption that

$$\varepsilon(\boldsymbol{r}) = \delta(\boldsymbol{r} - \boldsymbol{r'})S(\theta) \tag{2.24}$$

which means that there is only a perturbation at the scattering particle itself, at position $\boldsymbol{r'}$, and that we have no variation anywhere else in the medium. This assumption is also valid as we are only assuming single scattering. We include the amplitude function, denoted S because this function describes the outgoing scattered wave in relation to the incoming wave, i.e. it describes the perturbation ε. $\theta = \theta(x, y, z)$ here represents the angle of scattering of the wave front. This is discussed further in the succeeding section. This leaves (2.20) independent of $\boldsymbol{r}$ by the theorem for the three dimensional Dirac delta function, which states

$$\int_V f(\boldsymbol{r})\delta(\boldsymbol{r} - \boldsymbol{r'})dV = f(\boldsymbol{r'}) \tag{2.25}$$

where V is any volume that contains the point $\mathbf{r} = \mathbf{r}'$, where dV is an element of V expressed in terms of the components of $\mathbf{r}$.

Using (2.23) and (2.16) we can write (2.20) as

$$\begin{aligned}\chi(x, y, z) = \Re\Bigg\{ k^2 \int\int\int & \frac{\exp(ik(\sqrt{(L-x)^2 + \rho^2})}{4\pi\sqrt{(L-x)^2 + \rho^2}} \varepsilon(\sqrt{x^2 + \rho^2}) \frac{L}{\sqrt{x^2 + \rho^2}} \\ & \times \exp(ik(\sqrt{x^2 + \rho^2} - L)) dx dx dz \Bigg\}.\end{aligned} \tag{2.26}$$

and so by (2.25) the integral disappears and substituting in (2.24)we can re-write (2.20) as

$$\chi(x, y, z, \theta) = \Re\left\{ \frac{k^2}{4\pi} \frac{L}{x(L-x)} \exp\left(ik \frac{L(y^2 + z^2)}{2x(L-x)} \right) S(\theta) \right\}, \tag{2.27}$$

which represents the amplitude fluctuation of the electric field caused by a single scattering particle at position (x, y, z).

2.2 The Scattering Amplitude

We want to study the behaviour of microwaves when scattered by water droplets. In order to do this we need a way of describing what happens to the wave front as it travels through the droplet. Mie's scattering theory [6] describes the scattered electromagnetic wave in terms of an amplitude function. In this section we will express the scattering amplitude in terms of its associated Legendre polynomials as this will help later on with the numerical computations. We will not however, derive the amplitude functions from Maxwell's equations. This method of derivation involves a rigorous treatment of Maxwell's equations with the incident field being expressed in the form of spherical partial waves. We state the solution of the derivation below, which describes the scattering of electromagnetic waves by homogeneous spherical particles.

It is true that not all raindrops exhibit a perfectly spherical shape; however, for the most part a sphere can describe the shape of a raindrop, particularly for smaller drops, and so we omit non-spherical particles. Moreover, we are able to apply Mie's generalised scattering theory here because we are considering microwaves, which have a wavelength with order of magnitude of around $10^{-3} - 10^{-2}$m. The size of a raindrop is typically similar, in the region of around 10^{-3}. If we were considering particles with a size either much smaller or much larger than the wavelength we would have to use a more specialised form of Mie's theory for that particular case.

We are looking at the behaviour of spherical waves diverging from a point source. These waves behave locally like plane waves in the far-field region. This region is the only one we are interested in, as the behaviour of electromagnetic waves in the near-region is often very complex and difficult to predict, whereas in the far field waves exhibit more regular behaviour. For this study it is sufficient to only consider the behaviour of the far field as our path length is 0.5 km which is significantly larger than the near field region, and so the effect of any scattering in the near-field region can be neglected. The far-field in our case can be defined by the Fraunhofer distance

$$d_f \geq \frac{2D^2}{\lambda}, \tag{2.28}$$

where D represents the diameter of the antenna and λ the wavelength and d_f represents any distance away from the transmitter which can be considered in the 'far-field' region. In our case $d_f \geq 10$m.

The scattering amplitude which we have defined as $S(\theta)$ is a complex function, and describes the scattering in any direction. This scattering is described by four different amplitude functions, S_1, S_2, S_3 and S_4, where the overall scattering can be written in the form of a matrix.

$$\begin{pmatrix} E_\perp^S \\ E_\parallel^S \end{pmatrix} = \begin{pmatrix} S_2 & S_3 \\ S_4 & S_1 \end{pmatrix} \cdot \begin{pmatrix} E_\perp^I \\ E_\parallel^I \end{pmatrix} \frac{\exp(ik(|\boldsymbol{L} - \boldsymbol{r}|))}{|\boldsymbol{r}|}, \tag{2.29}$$

where S represents the scattered wave and I represents the incident wave, with $\perp$ and $\parallel$ representing the electric field components perpendicular and parallel to the plane of scattering, respectively. We show the idea in Figure 2.

Spherical particles have $S_3 = S_4 = 0$, and so the scattering depends only on two amplitude functions.

Mie scattering provides a solution to Maxwell's equation's to describe electromagnetic scattering. The solution can be written as an infinite series of spherical partial waves. With this we define S_1 and S_2 as

$$S_1(\theta) = \sum_{n=1}^{\infty} \frac{2n+1}{n(n+1)} \{a_n \pi_n(\cos\theta) + b_n(\theta)\tau_n(\cos\theta)\},$$

$$S_2(\theta) = \sum_{n=1}^{\infty} \frac{2n+1}{n(n+1)} \{b_n \pi_n(\cos\theta) + a_n(\theta)\tau_n(\cos\theta)\},$$

where

$$\pi_n(\cos(\theta)) = \frac{1}{\sin\theta} P_n^1(\cos\theta) = \frac{dP_n(\cos\theta)}{d\cos\theta},$$

$$\tau_n(\cos\theta) = \frac{d}{d\theta}(P_n^1(\cos\theta)) = \cos\theta \cdot \pi_n(\cos\theta) - \sin^2\theta \frac{d\pi_n(\cos\theta)}{d\cos\theta},$$

where P_n^1 are the first order Legendre Polynomials. This means that the scattered wave can be described by these Legendre Polynomials. Only $S_1(\theta)$ will be detected by the receiver, so with this we can then use the product rule to our final expression for $S_1(\theta)$ as

$$S_1(\theta) = \sum_{n=1}^{\infty} \frac{2n+1}{n(n+1)} \left\{ a_n \frac{P_n^1}{\sin\theta} - b_n \sin\theta \frac{dP_n^1(\cos\theta)}{d\cos\theta} \right\}. \tag{2.30}$$

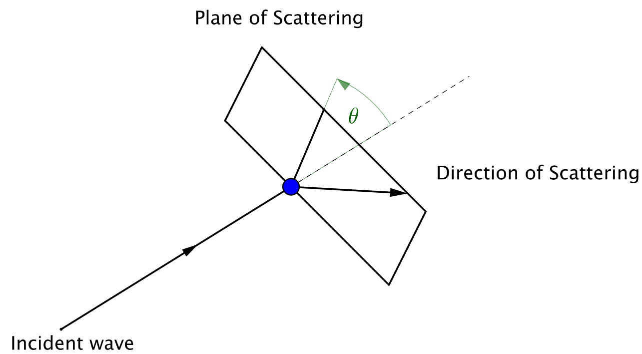

Figure 2: Plane of Scattering

The Mie-scattering coefficients are expressed in terms of Riccati-Bessel functions

$$a_n = \frac{\psi_n'(v)\psi_n(u) - m\psi_n'(v)\psi_n(u)}{\psi_n'(v)\zeta_n(u) - m\psi_n'(v)\zeta_n(u)} \tag{2.31}$$

and

$$b_n = \frac{m\psi_n'(v)\psi_n(u) - \psi_n(v)\psi_n'(u)}{m\psi_n'(v)\zeta_n{}'(u) - \psi_n(v)\zeta_n(u)}. \tag{2.32}$$

Here $u = ka$ and $v = mka$, where m is the complex refractive index of the water drop, k is the wavenumber and a is the radius of the water drop. We can define these Ricatti-Bessel functions as follows, with the Bessel functions of the first (J_α) and second kind (Y_α):

$$\psi_n(v) = \sqrt{\frac{\pi v}{2}} J_{n+1/2}(v) = v j_n(v) \tag{2.33}$$

and

$$\zeta_n(u) = -\sqrt{\frac{\pi v}{2}} Y_{n+1/2}(v) = -u y_n(u), \tag{2.34}$$

where j_n and y_n are the spherical Bessel functions of the first and second kind respectively. In order to compute these numerically one can make use of the recursive formula

$$j_{n+1}(v) = \frac{2n+1}{v} j_n(v) - j_{n-1}(z), \tag{2.35}$$

where the same relation holds for y_n, with

$$xj_0(v) = \sin(v), \qquad vj_1(v) = \frac{\sin(v)}{v} - \cos(v), \tag{2.36}$$

$$uy_0(u) = -\cos(u) \quad \text{and} \quad y_1(u) = \frac{-\sin(u)}{u} - \cos(u). \tag{2.37}$$

Using

$$\frac{d}{dv}\big(vj_n(v)\big) = \frac{1}{2}\big(vj_{n-1}(v) + j_n(v) - vj_{n+1}(v)\big), \tag{2.38}$$

the derivatives can also be computed. Note here that the derivative of $uy_n(u)$ has the identical form to the derivative of $vj_n(v)$.

2.3 The Covariance of Amplitude Fluctuations

We are taking the amplitude fluctuations caused by rainfall to be a wide-sense stationary (WSS) random process, which means that the mean and the autocovariance do not vary with respect to time. The autocovariance simply gives the covariance of the random process with itself, but at two different points in time. We can define this by

$$C_\chi(t_1, t_2) = \mathbb{E}[(\chi_{t_1} - \mu_{t_1})(\chi_{t_2} - \mu_{t_2})] \tag{2.39}$$

where μ_t defines the mean value of the random process at time t. The preceding equation is describing to what extent the amplitude fluctuations differ from one another at different time points. Because we have a WWS random process the covariance should only depend on the temporal separation $\tau = t_1 - t_2$. We can write this, assuming that the random process is known over an finite interval $[-T, T]$, as $T \to \infty$

$$C_\chi(\tau) = \frac{1}{T}\int_0^T \chi(t_1)\chi(t_2)dt \tag{2.40}$$

We will now bring in the concept of an ensemble average. An ensemble is defined as all possible configurations of the system; so naturally an ensemble average is the mean of these states. It is commonly denoted as $\langle\chi\rangle$, where

$$\langle\chi\rangle = \int_{-\infty}^{\infty} p(\chi)\chi d\chi \tag{2.41}$$

where $p(\chi)$ represents the probability density function of χ. Without prior measurements, it is not possible to know the exact pdf of the amplitude fluctuations. We now make the assumption that the ensemble average almost always equals the time average, i.e. the ensemble average and temporal average must converge as $T \to \infty$. This is known as the ergodic hypothesis. We can then write

$$\langle \chi(t) \rangle \approx \frac{1}{T} \int_0^T \chi(t) dt \tag{2.42}$$

and so we can re-write equation (2.40) as

$$C_\chi(\tau) = \langle \chi(t)\chi(t+\tau) \rangle \tag{2.43}$$

We can apply Taylor's hypothesis here, and say that the medium is frozen while the measurement of a raindrop is being taken, where the velocity of a falling raindrop, denoted v is taken to be constant during this interval. This is a reasonable assumption if the raindrop is at terminal velocity. Then the amplitude fluctuation caused by a single raindrop measured at time t_1 and time t_2 should be identical to the result measured at time t_1 but at a different point in space, defined by $v\tau$. This can be written as

$$C_\chi(\tau) = \langle \chi(x, y, z, t_1)\chi(x, y, z, t_1 + \tau) \rangle = \langle \chi(x, y, z, t_1)\chi(x, y, z - v\tau, t_1) \rangle \tag{2.44}$$

Another way of expressing this is to say that the temporal covariance is related to the spatial covariance by the terminal velocity of the raindrop v.

2.4 Fresnel Zones

Here we will introduce the concept of a Fresnel zone. These zones are crucial in determining whether any scattered wave will arrive in or out of phase with the waves propagating along the line of sight. A Fresnel Zone is a prolate ellipsoid, whose size is approximated by the following formula

$$F_n = \sqrt{\frac{n\lambda d_1 d_2}{d_1 + d_2}} \tag{2.45}$$

where F_n is the radius of the n^{th} Fresnel Zone, λ the wavelength of the signal and d_1,d_2 are the distances from either end to a point along the line of signal.

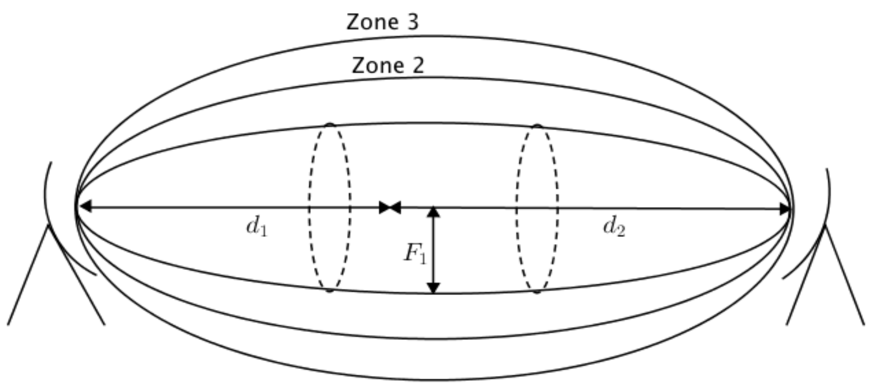

Figure 3: Fresnel Zones

There are an infinite number of Fresnel zones but only the signal contained within the first three Fresnel zones has any effect on the signal at the receiver. The first Fresnel zone is illustrated in Figure 3 above. Not all of the wave will propagate along the line of sight - the direct path between the signal and receiver- and some of these waves will be reflected by obstructions. When both the reflected and non-reflected wave reach the receiver, they may be out of phase due to the difference in path length, which will lead to destructive interference. This happens when the two signals are π radians apart. We get constructive interference when the two signals are 2π radians out of phase, and so the two signals will add together and will not negatively impact the output at the receiver. The first Fresnel zone radius is calculated so any objects causing reflections will arrive in phase with one another, the second zone will be out of phase, the third in phase and so on. The first Fresnel zone is the most significant in terms of signal strength and this is the one we will focus on in the succeeding section.

3 The Power Spectrum

Up until now we have given the reader some insight into spherical wave propagation and defined some statistical properties of microwaves passing through rainfall, such as the temporal covariance. We now introduce the Wiener-Khinchin theorem, a key theorem that will enable us to compare theoretical predictions with microwave link data, a key step in the retrieval of the drop size distribution.

3.1 The Wiener–Khinchin Theorem

Our expression for the temporal covariance function from section (2.3) is as follows

$$C_\chi(t) = \langle \chi(x,y,z)\chi(x,y,z-vt)\rangle,$$

so we have

$$C_\chi(t) = \int_{-\infty}^{\infty} \chi(x,y,z)\chi(x,y,z-vt)dz.$$

where we are able to integrate over the spatial variable z by Taylor's Hypothesis. Our amplitude function from expression (1.25), which we repeat below, is a complex number and so we can expand this expression as follows

$$\begin{aligned}\chi &= \Re\left\{\frac{k^2}{4\pi}\frac{L}{x(L-x)}\exp\left(ik\frac{L(y^2+z^2)}{2x(L-x)}\right)S(\theta)\right\}\\ &= \frac{k^2}{4\pi}\frac{L}{x(L-x)}\left(S_R\cos\left(\frac{L(y^2+z^2)}{2x(L-x)}\right) - S_I\sin\left(\frac{L(y^2+z^2)}{2x(L-x)}\right)\right),\end{aligned} \tag{3.1}$$

where S_R and S_I denote the real and imaginary part of the amplitude function $S(\theta)$ respectively. In the following equations we defined $S(\theta)$ in terms of x, y, z because θ will be dependent on these terms as we will see in (3.2). The temporal covariance function can then be written, where we expand to integrate over x and y as well to include the whole volume, as

$$\begin{aligned}C_\chi(t) =& \frac{k^4}{16\pi^2}\int_{-\infty}^{\infty}dx\int_{-\infty}^{\infty}dy\int_{-\infty}^{\infty}\beta^2\\ &\times\Bigg[S_R(x,y,z)S_R(x,y,z-vt)\cos\left(\frac{\beta}{2}(y^2+z^2)\right)\cos\left(\frac{\beta}{2}(y^2+(z-vt)^2)\right)\\ &- S_R(x,y,z)S_I(x.y,z-vt)\cos\left(\frac{\beta}{2}(y^2+z^2)\right)\sin\left(\frac{\beta}{2}(y^2+(z-vt)^2)\right)\\ &- S_R(x,y,z-vt)S_I(x,y,z-vt)\sin\left(\frac{\beta}{2}(y^2+z^2)\right)\cos\left(\frac{\beta}{2}(y^2+(z-vt)^2)\right)\\ &+ S_I(x,y,z)S_I(x,y,z-vt)\sin\left(\frac{\beta}{2}(y^2+z^2)\right)\sin\left(\frac{\beta}{2}(y^2+(z-vt)^2)\right)\Bigg]dz\end{aligned} \tag{3.2}$$

with

$$\beta = \frac{L}{x(L-x)}. \tag{3.3}$$

Using the trigonometric identity $\cos(u)\cos(v) = \frac{1}{2}[\cos(u-v) + \cos(u+v)]$ can simplify the above, giving

$$
\begin{aligned}
C_\chi(t) = &\frac{k^4}{16\pi^2}\int_{-\infty}^{\infty} dx \int_{-\infty}^{\infty} dy \int_{-\infty}^{\infty} \frac{\beta^2}{2} \\
&\times \Big[(S_R(x,y,z)S_R(x,y,z-vt) + S_I(x,y,z)S_I(x,y,z-vt))\cos(2zvt - (vt)^2) \\
&+ (S_R(x,y,z)S_R(x,y,z-vt) - S_I(x,y,z)S_I(x,y,z-vt))\cos(2y^2 + 2z^2 - 2zvt + (vt)^2) \\
&- (S_R(x,y,z)S_I(x,y,z-vt) - S_R(x,y,z-vt)S_i(x,y,z)\sin(2y^2 + 2z^2 - 2zvt + (vt)^2) \\
&+ (S_R(x,y,z-vt)S_I(x,y,z) - S_R(x,y,z)S_i(x,y,z-vt))\sin(2zvt - (vt)^2)\Big] dz.
\end{aligned} \tag{3.4}
$$

We now introduce the Wiener-Khinchin Theorem, which is crucial in order for us to compare theoretical predictions with real data. Here we consider a time series $\mu(t)$ for $t \to \infty$. The temporal covariance function for this time series at time t and time $t+\tau$ is

$$
C_\tau(t) = \frac{1}{T}\int_0^\infty \mu(t)\mu(t+\tau)dt \tag{3.5}
$$

The Fourier transform of $\mu : \mathbb{R} \to \mathbb{C}$ is defined as

$$
\hat{\mu}(f) = \int_{-\infty}^{\infty} \mu(\tau)e^{-i2\pi f\tau}d\tau \tag{3.6}
$$

for $f \in \mathbb{R}$. Now we introduce the function $P(f)$, which denotes the power spectral density. This describes the distribution of power as a function of frequency, per unit of frequency. This is defined as

$$
\mathcal{P}(f) \simeq |\hat{\mu}(f)|^2 \tag{3.7}
$$

for a short time interval t. The units of the power spectrum are watts per hertz (W/Hz). We note that the power spectral density is usually expressed in the limit as $t \to \infty$; however, we use the definition of the energy spectral density here as were are considering finite time. The Wiener-Khinchin theorem then states that if μ is a wide sense stationary process, where its temporal covariance function exists and is finite for all $\tau \in t$, then we can define the Fourier transform of it's temporal covariance function as the power spectrum of μ.

This can easily be seen by the fact that the temporal covariance function, defined as $C_\tau = x(t) * x(\tau)$ is the convolution of the signal at two different time points. A convolution in the time domain is a multiplication in the frequency domain, and at two different points in the time domain is the same as its complex conjugate in the frequency domain. This leads to

$$
\mathcal{F}\{C_\tau(t)\} = \mathcal{F}\{x(t) * x(\tau)\} = \mathcal{F}\{x(t)\}\mathcal{F}\{x(\tau)\} = Y(f)Y^*(f) = |Y(f)|^2 \tag{3.8}
$$

where $Y(f) = \int_{-\infty}^{\infty} x(t)e^{-i2\pi ft}dt$.

Using equation (3.6), we can write the Fourier transform of the autocovariance function as

$$
\begin{aligned}
\mathcal{F}_\chi(f) &= \int_{-\infty}^{\infty} e^{-i2\pi ft} C_\chi(t) dt \\
&= \frac{k^4}{16\pi^2} \int_{-\infty}^{\infty} dx \int_{-\infty}^{\infty} dy \int_{-\infty}^{\infty} e^{-i2\pi ft} \int_{-\infty}^{\infty} \frac{\beta^2}{2} \\
&\times \Big[(S_R(x,y,z)S_R(x,y,z-vt) + S_I(x,y,z)S_I(x,y,z-vt)) \cos(2zvt - (vt)^2) \\
&+ (S_R(x,y,z)S_R(x,y,z-vt) - S_I(x,y,z)S_I(x,y,z-vt)) \cos(2y^2 + 2z^2 - 2zvt + (vt)^2) \\
&- (S_R(x,y,z)S_I(x,y,z-vt) - S_R(x,y,z-vt)S_i(z) \sin(2y^2 + 2z^2 - 2zvt + (vt)^2) \\
&+ (S_R(x,y,z-vt)S_I(z) - S_R(x,y,z)S_i(x,y,z-vt)) \sin(2zvt - (vt)^2) \Big] dz dt
\end{aligned} \tag{3.9}
$$

3.2 Angle of scattering

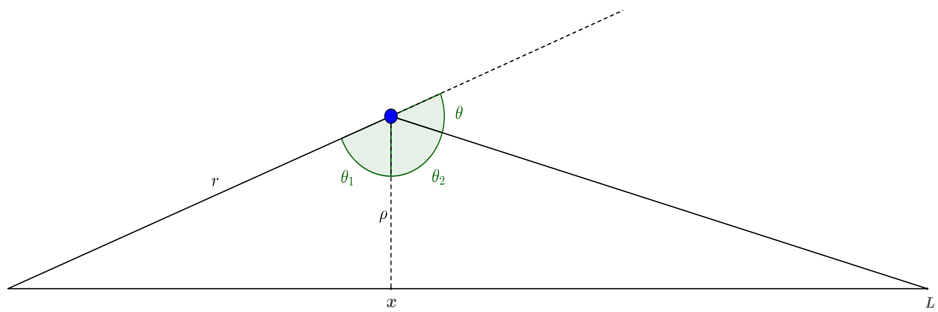

Figure 4: Angle of scattering

We will now define our scattering angle θ which we have shown in figure 4. We are only interested in the far field solution and so the transverse coordinate x will be a lot larger than y and z we can make the assumption that $r \approx x$ and $R \approx L - x$. This will greatly simply our expression. We define our scattering angle θ as

$$\begin{aligned} \theta &= \pi - \theta_1 - \theta_2 \\ &= \pi - \arccos\left(\frac{\sqrt{y^2 + z^2}}{x}\right) - \arccos\left(\frac{\sqrt{y^2 + z^2}}{L - x}\right) \end{aligned} \tag{3.10}$$

Because we are considering the far-field solution, both terms inside the brackets will be smaller than unity, we can use the approximation $\arccos(\xi) = \frac{\pi}{2} - \xi$, with $|\xi| \ll 1$. This leads to

$$\theta = \beta(\sqrt{y^2 + z^2}) \tag{3.11}$$

where $\beta = \frac{L}{x(L-x)}$ as defined in (3.3).

3.3 The Method of Stationary Phase

We will introduce the following substitution in order to gain some idea of how the integral in (3.9) behaves in the limit $t \to \infty$. In order to factorise the term inside of the trigonometric functions in

(3.9) we can write

$$\begin{aligned}
\gamma &= \frac{2k}{\beta}, \\
\bar{v} &= \beta v, \\
\bar{y} &= \beta y \qquad \text{and} \\
\bar{z} &= \beta z.
\end{aligned} \tag{3.12}$$

$$\begin{aligned}
\mathcal{F}_\chi(f) = \frac{k^4}{16\pi^2}\int_{-\infty}^{\infty} dx \int_{-\infty}^{\infty} d\bar{y} \int_{-\infty}^{\infty} e^{-i2\pi f t} \int_{-\infty}^{\infty} \frac{1}{2}\Big[&(S_R(\sqrt{\bar{y}^2+\bar{z}^2})S_R(\sqrt{\bar{y}^2+(\bar{z}-\bar{v}t)^2}) \\
&- S_I(\sqrt{\bar{y}^2+\bar{z}^2})S_I(\sqrt{\bar{y}^2+(\bar{z}-\bar{v}t)^2}))\cos(\gamma(\bar{y}^2+\bar{z}^2-\bar{z}\bar{v}t+(\bar{v}t)^2/2)) \\
&+ (S_R(\sqrt{\bar{y}^2+\bar{z}^2})S_R(\sqrt{\bar{y}^2+(\bar{z}-\bar{v}t)^2}) + S_I(\sqrt{\bar{y}^2+\bar{z}^2})S_I(\sqrt{\bar{y}^2+(\bar{z}-\bar{v}t)^2})) \\
&\times \cos(\gamma(\bar{z}\bar{v}t-(\bar{v}t)^2/2)) \\
&- (S_R(\sqrt{\bar{y}^2+\bar{z}^2})S_I(\sqrt{\bar{y}^2+(\bar{z}-\bar{v}t)^2}) + S_R(\sqrt{\bar{y}^2+(\bar{z}-\bar{v}t)^2})S_I(\sqrt{\bar{y}^2+\bar{z}^2})) \\
&\times \sin(\gamma(\bar{y}^2+\bar{z}^2-\bar{z}\bar{v}t+(\bar{v}t)^2/2)) \\
&+ (S_R(\sqrt{\bar{y}^2+(\bar{z}-\bar{v}t)^2})S_I(\sqrt{\bar{y}^2+\bar{z}^2}) - S_R(\sqrt{\bar{y}^2+\bar{z}^2})S_I(\sqrt{\bar{y}^2+(\bar{z}-\bar{v}t)^2})) \\
&\times \sin(\gamma(\bar{z}\bar{v}t-(\bar{v}t)^2/2))\Big] d\bar{z}dt.
\end{aligned} \tag{3.13}$$

We can see here that the trigonometric functions involved in (3.13) oscillate rapidly compared with the associated Legendre polynomials involved in the amplitude function. This is clear because of the factor $\gamma \gg 1$ inside the cosine and sine function. The rapid oscillations of the trigonometric functions means that the integrand will average out to almost zero. An anomaly to this happens when the term inside the trigonometric function is stationary. We can show the idea with the following integral, of the form

$$F(u) = \int_{\mathbb{R}} f(t)\exp(iug(t))dt, \tag{3.14}$$

where the role of $f(t)$ is to guarantee convergence, and $u \in \mathbb{R}$ is considered as $u \to \infty$. (3.14) resembles the form of the integrals in (3.13) and we suppose that $g'(t_0) = 0$, where $t_0 \in (a, b)$, and that $g'(t_0) \neq 0$ in the rest of the interval. We can also assume that $g''(t_0) \neq 0$ and $f'(t_0) \neq 0$. The integral can then be approximated by finding all points where the derivative with respect to t is zero, and evaluating in the neighbourhood of these points. This is known as the *method of stationary phase*.

We can re-write (3.14) as

$$F(u) = \exp(iug(t_0))\int_{\mathbb{R}} f(t)\exp(iu[g(t)-g(t_0)])dt. \tag{3.15}$$

Now take $\phi = ug(t)$, which is the phase term, and expand this as a Taylor series about $g(t)$, which gives us $g(t) = g(t_0) + \frac{g''(t_0)}{2!}(t-t_0)^2 + \mathcal{O}[(t-t_0)^3]$. Substituting this in we have

$$\begin{aligned} F(u) &\approx \exp(iug(t_0)) \int_{t_0-\epsilon}^{t_0+\epsilon} f(t) \exp(iu[g(t)-g(t_0)])dt \\ &\approx f(t_0)\exp(iug(t_0)) \int_{t_0-\epsilon}^{t_0+\epsilon} \exp\left(\frac{iu}{2} g''(t_0)(t-t_0)^2\right) dt \\ &\approx f(t_0)\exp(iug(t_0)) \int_{-\infty}^{\infty} \exp\left(\frac{iu}{2} g''(t_0)p^2\right) dp \\ &= f(t_0)\exp(iug(t_0)) \sqrt{\frac{2\pi i}{ug''(t_0)}} \\ &= f(t_0)\exp(iug(t_0)) \mp \frac{i\pi}{4} \sqrt{\frac{2\pi}{u|g''(t_0)|}} \end{aligned} \tag{3.16}$$

where $p = t - t_0$. We have used the identity $\sqrt{\frac{\pi}{-ix}} = e^{\frac{i\pi}{4}} \frac{\sqrt{\pi}}{\sqrt{x}}$ and the plus and minus signs correspond to $g''(t_0) > 0$ and $g''(t_0) < 0$ respectively. We note before evaluating the Fourier transform of the amplitude fluctuations in this way that it is assumed by this method that the stationary point $t_0 \in \mathbb{R}$ is in t-space and so we can evaluate the integral at $\cos(ug(t))$, rather than $\exp(iug(t))$.

For readability we will split equation (3.13) into four integrals and tackle them separately. We will label them $\mathcal{F}_n$ for $n \in [1,4]$, where $\sum_{n=1}^{4} \mathcal{F}_n(f) = \mathcal{F}_\chi(f)$. Our first integral will be

$$\begin{aligned} \mathcal{F}_1(f) = \frac{k^4}{16\pi^2} \int_{-\infty}^{\infty} dx \int_{-\infty}^{\infty} d\bar{y} \int_{-\infty}^{\infty} e^{-i2\pi f t} \int_{-\infty}^{\infty} \frac{1}{2} \Big[(S_R(\sqrt{\bar{y}^2+\bar{z}^2}) S_R(\sqrt{\bar{y}^2+(\bar{z}-\bar{v}t)^2}) \\ - S_I(\sqrt{\bar{y}^2+\bar{z}^2}) S_I(\sqrt{\bar{y}^2+(\bar{z}-\bar{v}t)^2})) \cos(\gamma(\bar{y}^2+\bar{z}^2-\bar{z}\bar{v}t+(\bar{v}t)^2/2)) \Big] d\bar{z}dt. \end{aligned} \tag{3.17}$$

Evaluating the above integral with respect to t could become quite complicated and so we introduce another substitution $z' = \bar{v}t - \bar{z}$ in order to reduce the expression within the amplitude function S.

$$\begin{aligned} \mathcal{F}_1(f) = \int_{-\infty}^{\infty} \frac{k^4}{16\pi^2} \frac{2}{\bar{v}} \int_{-\infty}^{\infty} d\bar{y} \int_{-\infty}^{\infty} e^{-2\pi f \frac{\bar{z}}{\bar{v}} i} \int_{0}^{\infty} (S_R(\sqrt{\bar{y}^2+\bar{z}^2}) S_R(\sqrt{\bar{y}^2+z'^2}) \\ - S_I(\sqrt{\bar{y}^2+\bar{z}^2}) S_I(\sqrt{\bar{y}^2+z'^2})) \cos\left(2\pi f \frac{z'}{\bar{v}}\right) \cos(\gamma(\bar{y}+\bar{z}/2+z'^2/2)) dx d\bar{z} dz'. \end{aligned} \tag{3.18}$$

We have changed the limit of the integral with respect to z' because the integral is symmetric around $z' = 0$. We can then use $\cos(u)\cos(v) = \frac{1}{2}[\cos(u-v)+\cos(u+v)]$ in order to determine the stationary phase point for z'. This will give

$$\begin{aligned} \cos\left(2\pi f \frac{z'}{\bar{v}}\right) \cos(\gamma(\bar{y}+\bar{z}/2+z'^2/2)) = \frac{1}{2} \Bigg(\cos\Bigg(\gamma[\bar{y}+\bar{z}^2/2+z'^2/2] \\ + \frac{2\pi f z'}{\bar{v}} \Bigg) + \cos\left(\gamma[\bar{y}+\bar{z}^2/2+z'^2/2] - \frac{2\pi f z'}{\bar{v}} \right) \Bigg) \end{aligned} \tag{3.19}$$

where we have both $g(z') = \gamma[\bar{y}+\bar{z}^2/2+z'^2/2] + \frac{2\pi f z'}{\bar{v}}$ and $g(z') = \gamma[\bar{y}+\bar{z}^2/2+z'^2/2] - \frac{2\pi f z'}{\bar{v}}$. We note that we only have a stationary point within the second term because the first term will give a negative stationary point which is out of bounds for z'. By doing this we can recognize from $g'(z_0') = \frac{-2\pi f z_0'}{\bar{v}} - \gamma\bar{z}$ that there is a stationary point at $z_0' = \frac{2\pi f}{\gamma\bar{v}}$ with $g''(z_0') = \gamma > 0$. $\mathcal{F}_1$ now takes the form

$$\begin{aligned}\mathcal{F}_1(f) = \int_{-\infty}^{\infty} \sqrt{\frac{2\pi}{\gamma}} \frac{k^4}{16\pi^2} \frac{2}{\bar{v}} \int_{-\infty}^{\infty} e^{2\pi f i \frac{\bar{z}}{\bar{v}}} d\bar{z} \int_{-\infty}^{\infty} \Bigg(S_R(\sqrt{\bar{y}^2 + \bar{z}^2}) S_R\Bigg(\sqrt{\bar{y}^2 + \left(\frac{2\pi f}{\gamma\bar{v}}\right)^2}\Bigg) \\ - S_I(\sqrt{\bar{y}^2 + \bar{z}^2}) S_I\Bigg(\sqrt{\bar{y}^2 + \left(\frac{2\pi f}{\gamma\bar{v}}\right)^2}\Bigg)\Bigg) \cos\left(\gamma(\bar{y} + \bar{z}/2) + \frac{\pi}{4} - \left(\frac{2\pi f}{\bar{v}}\right)^2 \left(\frac{1}{2\gamma}\right)\right) dx d\bar{y}.\end{aligned} \tag{3.20}$$

We will first evaluate (3.20) with respect to $\bar{y}$ as it can be easily seen that there will be a stationary phase point at $\bar{y}_0 = 0$, where again the integral is symmetric with respect to $\bar{y}$. Here we have $g'(\bar{y}_0) = 2\gamma\bar{y}$ and $g''(\bar{y}_0) = 2\gamma$.

Using the relation $\cos(\frac{\pi}{2} - u) = \sin(u)$ gives

$$\begin{aligned}\mathcal{F}_1(f) = \int_{-\infty}^{\infty} \sqrt{\frac{\pi}{\gamma}} \sqrt{\frac{2\pi}{\gamma}} \frac{k^4}{16\pi^2} \frac{2}{\bar{v}} \int_{-\infty}^{\infty} \Bigg(S_R(\bar{z}) S_R\left(\frac{2\pi f}{\gamma\bar{v}}\right) \\ - S_I(\bar{z}) S_I\left(\frac{2\pi f}{\gamma\bar{v}}\right)\Bigg) \cos\left(2\pi f \frac{\bar{z}}{\bar{v}}\right) \sin\left(\frac{\gamma\bar{z}}{2} - \left(\frac{2\pi f}{\bar{v}}\right)^2 \left(\frac{1}{2\gamma}\right)\right) dx d\bar{z}.\end{aligned} \tag{3.21}$$

In a similar way to above the stationary phase point for $\bar{z}$ is found to be $\bar{z}_0 = \frac{2\pi f}{\gamma\bar{v}}$. This reduces the preceding equation to

$$\mathcal{F}_1(f) = \int_{-\infty}^{\infty} \sqrt{\frac{\pi}{\gamma}} \frac{2\pi}{\gamma} \frac{k^4}{16\pi^2} \frac{1}{\bar{v}} \left(S_R^2\left(\frac{2\pi f}{\gamma\bar{v}}\right) + S_I^2\left(\frac{2\pi f}{\gamma\bar{v}}\right)\right) \sin\left(\frac{\pi}{2} - \left(\frac{\pi f}{\bar{v}}\right)^2 \left(\frac{2}{\gamma}\right)\right) dx. \tag{3.22}$$

Using (3.12) we can write

$$\mathcal{F}_1(f) = \int_{-\infty}^{\infty} \frac{k^{5/2}}{8\pi^2} \frac{1}{v} \sqrt{\frac{L}{\pi x(L-x)}} \left(S_R^2\left(\frac{2\pi f}{\gamma\bar{v}}\right) + S_I^2\left(\frac{2\pi f}{\gamma\bar{v}}\right)\right) \sin\left(\frac{\pi}{2} - 2\left(\frac{\pi f}{v}\right)^2 \frac{x(L-x)}{kL}\right) dx. \tag{3.23}$$

Next we will evaluate $\mathcal{F}_2(f)$ with

$$\begin{aligned}\mathcal{F}_2(f) &= \frac{k^4}{16\pi^2} \int_{-\infty}^{\infty} dx \int_{-\infty}^{\infty} d\bar{y} \int_{-\infty}^{\infty} e^{-i2\pi f t} \int_{-\infty}^{\infty} \frac{1}{2} \Big[(S_R(\sqrt{\bar{y}^2 + \bar{z}^2}) S_R(\sqrt{\bar{y}^2 + (\bar{z} - \bar{v}t)^2}) \\ &+ S_I(\sqrt{\bar{y}^2 + \bar{z}^2}) S_I(\sqrt{\bar{y}^2 + (\bar{z} - \bar{v}t)^2})) \cos(\gamma(\bar{z}\bar{v}t - (\bar{v}t)^2/2) \Big] d\bar{z} dt \\ &= \frac{k^4}{8\pi^2} \int_{-\infty}^{\infty} dx \int_{-\infty}^{\infty} d\bar{y} \int_{-\infty}^{\infty} e^{-i2\pi f t} \int_{0}^{\infty} \frac{1}{2} \Big[(S_R(\sqrt{\bar{y}^2 + \bar{z}^2}) S_R(\sqrt{\bar{y}^2 + (\bar{z} - \bar{v}t)^2}) \\ &+ S_I(\sqrt{\bar{y}^2 + \bar{z}^2}) S_I(\sqrt{\bar{y}^2 + (\bar{z} - \bar{v}t)^2})) \\ &\times (\cos(\gamma(\bar{z}\bar{v}t - (\bar{v}t)^2/2) + 2\pi f t) + \cos(\gamma(\bar{z}\bar{v}t - (v't)^2/2) - 2\pi f t)) \Big] d\bar{z} dt.\end{aligned} \tag{3.24}$$

A stationary phase point exists for the second term, with $g'(t_0) = \gamma\bar{z}\bar{v} - \gamma\bar{v}^2 t - 2\pi f$ and so

$t_0 = \frac{\bar{z}}{\bar{v}} - \frac{2\pi f}{\gamma \bar{v}^2}$, with $g''(t_0) = -\gamma \bar{v}^2 < 0$. This gives

$$\mathcal{F}_2(f) = \int_{-\infty}^{\infty} dx \int_{-\infty}^{\infty} d\bar{y} \int_{-\infty}^{\infty} \sqrt{\frac{2\pi}{\gamma \bar{v}^2}} \frac{k^4}{16\pi^2} \int_{-\infty}^{\infty} e^{-i2\pi f t} d\bar{z} \int_0^{\infty} \frac{1}{2} \Bigg[(S_R(\sqrt{\bar{y}^2 + \bar{z}^2}) S_R\left(\sqrt{\bar{y}^2 + \left(\frac{2\pi f}{\gamma \bar{v}}\right)^2}\right)$$
$$+ S_I(\sqrt{\bar{y}^2 + \bar{z}^2}) S_I\left(\sqrt{\bar{y}^2 + \left(\frac{2\pi f}{\gamma \bar{v}}\right)^2}\right)$$
$$\times \cos\left(\frac{\gamma \bar{z}^2}{2} + \left(\frac{2\pi f \bar{z}}{\bar{v}}\right) + \left(\frac{2\pi f}{\bar{v}}\right)^2 \left(\frac{1}{2\gamma}\right) - \frac{\pi}{4}\right)\Bigg] d\bar{z} dt. \tag{3.25}$$

Evaluating the preceding integral with respect to $\bar{z}$, we find that $g(\bar{z}_0) = \frac{\alpha \bar{z}^2}{2} - \frac{2\pi f \bar{z}}{\bar{v}} + \frac{2\pi f^2}{2\gamma \bar{v}^2} - \frac{\pi}{4}$, $g'(\bar{z}_0) = \gamma \bar{z} - \frac{2\pi f}{\bar{v}}$, $g''(\bar{z}_0) = \alpha > 0$ and $\bar{z}_0 = \frac{2\pi f}{\gamma \bar{v}}$. Substituting back in, we find that $g(\bar{z}_0) = 0$. As everything cancels we have $\cos(0) = 1$. This leaves us with

$$\begin{aligned} \mathcal{F}_2(f) &= \int_{-\infty}^{\infty} \sqrt{\frac{2\pi}{\gamma \bar{v}^2}} \sqrt{\frac{2\pi}{\gamma}} \frac{k^4}{16\pi^2} \int_{-\infty}^{\infty} S_R^2\left(\sqrt{\bar{y}^2 + \left(\frac{\pi f}{kv}\right)^2}\right) + S_I^2\left(\sqrt{\bar{y}^2 + \left(\frac{\pi f}{kv}\right)^2}\right) dx d\bar{y} \\ &= \frac{k^3}{16\pi v} \int_{-\infty}^{\infty} \int_{-\infty}^{\infty} S_R^2\left(\sqrt{\bar{y}^2 + \left(\frac{\pi f}{kv}\right)^2}\right) + S_I^2\left(\sqrt{\bar{y}^2 + \left(\frac{\pi f}{kv}\right)^2}\right) dx d\bar{y}. \end{aligned} \tag{3.26}$$

When equation (3.26) is written in the form of (2.30), this is a very difficult integral to evaluate. We will first change the variable of integration to θ, where $\theta = \sqrt{\bar{y}^2 + \left(\frac{2\pi f}{\gamma \bar{v}}\right)^2}$. This gives

$$\mathcal{F}_2(f) = \frac{k^3}{16\pi v} \int_{-\infty}^{\infty} \int_{\frac{\pi f}{kv}}^{\infty} (S_R^2(\theta) + S_I^2(\theta)) \frac{\theta}{\sqrt{\theta^2 - \left(\frac{\pi f}{kv}\right)^2}} dx d\theta. \tag{3.27}$$

There is still an infinite upper limit on this integral that we want to remove. We can reduce the limit of this integral and only consider the scattering angles θ, which ensures that the scattering wave remains inside the first Fresnel zone. As the Fresnel zone is a prolate ellipsoid the equation can be written as follows, where we take our origin of coordinates to be at the location of the transmitter, with the origin of the ellipsoid to be at $(\frac{L}{2}, 0, 0)$;

$$\frac{(x - \frac{L}{2})^2}{\left(\frac{L}{2}\right)^2} + \frac{y^2}{F_1^2} + \frac{z^2}{F_1^2} = 1, \tag{3.28}$$

where F_1 is the radius of the first Fresnel zone as defined in (2.45). If we only consider the projection of the ellipsoid on the $xy-$plane we have

$$\frac{(x - \frac{L}{2})^2}{\left(\frac{L}{2}\right)^2} + \frac{y^2}{F_1^2} \leq 1. \tag{3.29}$$

Rearranging for y, which we transform back into $\bar{y}$, gives

$$\bar{y} \leq \beta \sqrt{F_1^2 - \left(\frac{F_1 x}{\frac{L}{2}}\right)^2}. \tag{3.30}$$

From the relation $\theta = \sqrt{\bar{y}^2 + \left(\frac{2\pi f}{\gamma \bar{v}}\right)^2}$ we have

$$\bar{y} = \sqrt{\theta^2 - \left(\frac{\pi f}{kv}\right)^2}. \tag{3.31}$$

Combining (3.30) and (3.31) gives

$$\theta \leq \sqrt{\left(\frac{\pi f}{kv}\right)^2 + \beta^2 \left(F_1^2 - \left(\frac{F_1 x}{\frac{L}{2}}\right)^2\right)}, \tag{3.32}$$

so equation (3.27) can then be re-written as

$$\mathcal{F}_2(f) = \frac{k^3}{16\pi v} \int_{-\infty}^{\infty} \int_{\frac{\pi f}{kv}}^{h(f,x)} (S_R^2(\theta) + S_I^2(\theta)) \frac{\theta}{\sqrt{\theta^2 - \left(\frac{\pi f}{kv}\right)^2}} dx d\theta, \tag{3.33}$$

where

$$h(f,x) = \sqrt{\left(\frac{\pi f}{kv}\right)^2 + \beta^2 \left(F_1^2 - \left(\frac{F_1 x}{\frac{L}{2}}\right)^2\right)}. \tag{3.34}$$

The remaining two integrals, $\mathcal{F}_3$ and $\mathcal{F}_4$, can be evaluated in a very similar way. For $\mathcal{F}_3$, we have

$$\begin{aligned} \mathcal{F}_3(f) = \frac{k^4}{16\pi^2} & \int_{-\infty}^{\infty} dx \int_{-\infty}^{\infty} d\bar{y} \int_{-\infty}^{\infty} e^{-i2\pi f t} \int_{-\infty}^{\infty} \frac{1}{2} \\ & \times \left(S_R(\sqrt{\bar{y}^2 + \bar{z}^2}) S_I(\sqrt{\bar{y}^2 + (\bar{z} - \bar{v}t)^2}) + S_R(\sqrt{\bar{y}^2 + (\bar{z} - \bar{v}t)^2}) S_I(\sqrt{\bar{y}^2 + \bar{z}^2} \right) \\ & \times \sin(\gamma(\bar{y}^2 + \bar{z}^2 - \bar{z}\bar{v}t + (\bar{v}t)^2/2) d\bar{z} dt. \end{aligned} \tag{3.35}$$

The trigonometric function is of almost identical form to that of $\mathcal{F}_1$, and so we can evaluate it in the same way. This will give

$$\mathcal{F}_3(f) = -\int_{-\infty}^{\infty} \frac{k^{5/2}}{8\pi^2} \frac{1}{v} \sqrt{\frac{L}{\pi x (L-x)}} \left(S_R\left(\frac{2\pi f}{\gamma \bar{v}}\right) S_I\left(\frac{2\pi f}{\gamma \bar{v}}\right)\right) \cos\left(\frac{\pi}{2} - 2\left(\frac{\pi f}{v}\right)^2 \frac{x(L-x)}{kL}\right)\bigg). \tag{3.36}$$

By following a similar method to that of $\mathcal{F}_2$, we know that $S_R(\sqrt{\bar{y}^2 + \bar{z}^2}) = (S_R(\sqrt{\bar{y}^2 + (\bar{z} - \bar{v}t)^2}))$, with the same result for S_I and so $\mathcal{F}_4(f) = 0$. Our final result for the analytical expression for the Fourier transform of amplitude fluctuations caused by raindrops is

$$\begin{aligned} \mathcal{F}_\chi(f) = A \Bigg[& \frac{k^{5/2}}{8\pi^2} \frac{1}{v} \int_0^L \sqrt{\frac{L}{\pi x (L-x)}} \left(S_R^2\left(\frac{2\pi f}{\gamma \bar{v}}\right) + S_I^2\left(\frac{2\pi f}{\gamma \bar{v}}\right)\right) \\ & \times \sin\left(\frac{\pi}{2} - 2\left(\frac{\pi f}{v}\right)^2 \frac{x(L-x)}{kL}\right)\bigg) - 2 S_R\left(\frac{2\pi f}{\gamma \bar{v}}\right) S_R\left(\frac{2\pi f}{\gamma \bar{v}}\right) \\ & \times \cos\left(\frac{\pi}{2} - 2\left(\frac{\pi f}{v}\right)^2 \frac{x(L-x)}{kL}\right)\bigg)\bigg) \\ & + \frac{k^3}{16\pi v} \int_{\frac{\pi f}{kv}}^{h(f,x)} (S_R^2(\theta) + S_I^2(\theta)) \frac{\theta}{\sqrt{\theta^2 - \left(\frac{\pi f}{kv}\right)^2}} d\theta dx \Bigg], \end{aligned} \tag{3.37}$$

where we have limited the range of integration for the spatial variable x to $\frac{2D^2}{\lambda} < x < L - \frac{2D^2}{\lambda}$ to account for any scattering between the transmitter and receiver. Any scattering where $x > L$ would be back scattering, which we are not taking into consideration. $\frac{2D^2}{\lambda}$ defines the far-field region, from (2.28). We show this result numerically in the following plots, where we approximated the integral by expressing it as a Riemann sum. It is important to note here that the amplitude function $S(\theta)$ is a function of f, and so this needs to be taken into account. Also note that we have included the constant A, which represents the number density. We include here the number density of raindrops for a mono-disperse distribution because we want now a realistic approximation of total fluctuations caused by all the raindrops causing fluctuations that are seen at the receiver, and so we include the number density. It is commonly expressed as

$$A = \frac{R}{4.8\pi \times 10^6 a^3 v}, \tag{3.38}$$

where R is the rainrate, v is the terminal velocity of a raindrop, and a the radius.

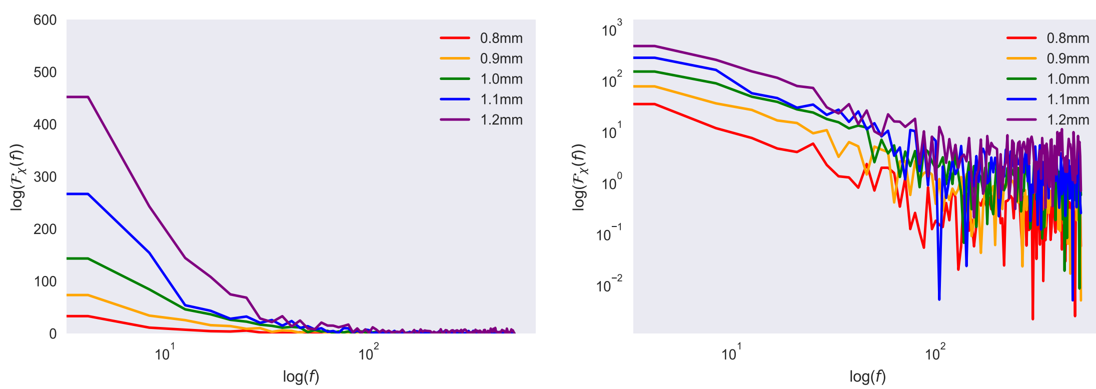

(a) Logarithmic x-axis.

(b) Logarithmic x and y-axis.

Figure 5: The Fourier Transform for a monodisperse distribution, for a range of drop sizes. Here the rain rate is taken to be 5mm/h.

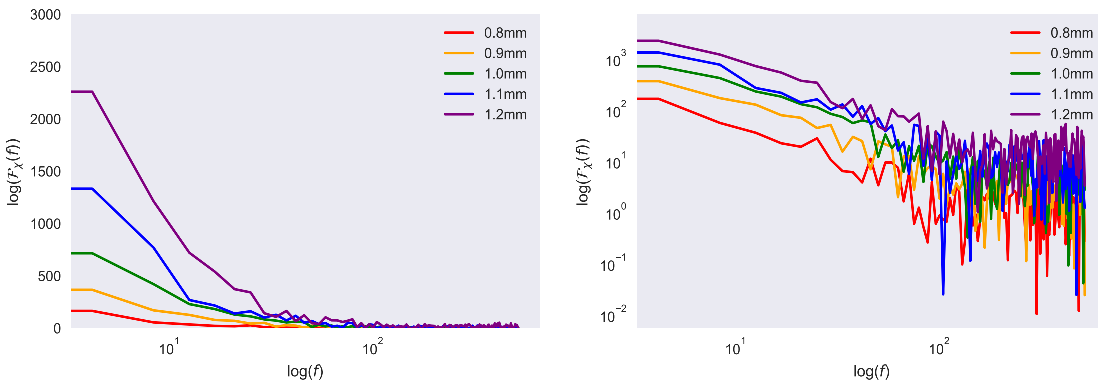

(a) Logarithmic x-axis.

(b) Logarithmic x and y-axis.

Figure 6: The Fourier Transform for a monodisperse distribution, for a range of drop sizes. Here the rain rate is taken to be 25mm/h.

4 The Data

4.1 Microwave Links

Microwave links are a type of communication system with a huge range of uses. These include cellular communication networks as well as wireless internet access. The main reason they are used in many communication services is due to the huge amount of information they can carry at very high speeds. Moreover, despite any attenuation in the signal, mainly due to rainfall and turbulence, the transmission is not disrupted.

4.2 Experimental Set up

The data was collected from an experiment set up at the Chilbolton Observatory in Southern England. The experiment recorded data from a logarithmic receiver and a linear receiver. Only data from the logarithmic receiver is relevant for this study, as we saw earlier when we derived the log amplitude fluctuations. In the data collection process the transmitter and receiver were positioned 500m away from one another, and placed 4m above the ground. The carrier frequency used was 26GHz, and the sampling frequency 25Hz. The transmit power of the link was 3dBm. Data was collected over a five month period, from September 2009 to January 2010.

(a) 26Ghz and 38 Ghz Transmitter at Chilbolton Oberservatory

(b) Birds Eye View with the yellow line showing the path of the microwave links

As previously mentioned, current research being done on using microwave links for rainfall estimation looks at attenuation of the signal. We show here the link signal data and rainfall intensity for two different days. We firstly plot the rainfall intensity measured with a rain gauge, as well as the power output at the receiver, for 6^{th}October 2009, which is shown in figure (8). In figure (9) we zoom in on a time period where there is large amount of rainfall. We also show a similar result for 23^{rd} December 2009. It is clear to see that there is a definite relation between rainfall intensity and signal attenuation.

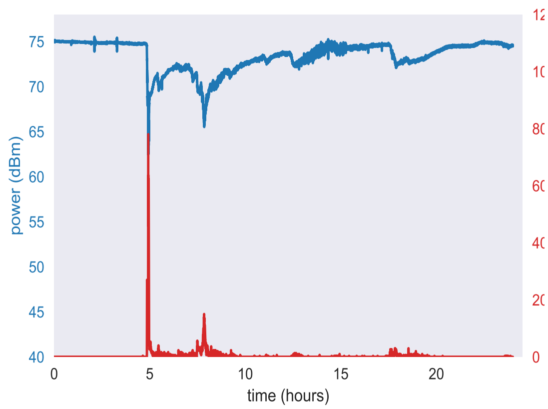

Figure 8: 06/10/2006

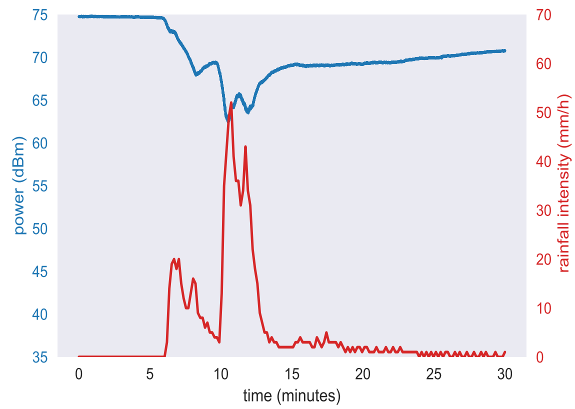

Figure 9: 06/10/2009, 04:45-05:15

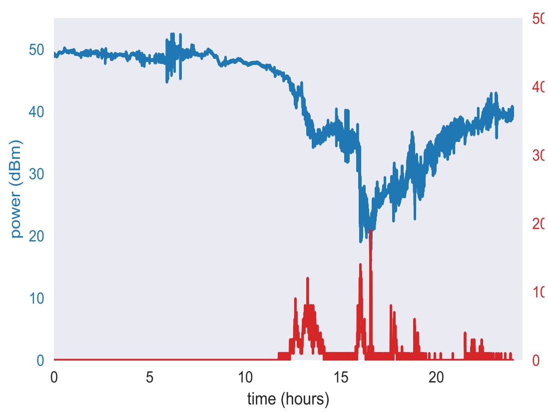

Figure 10: 23/12/2009

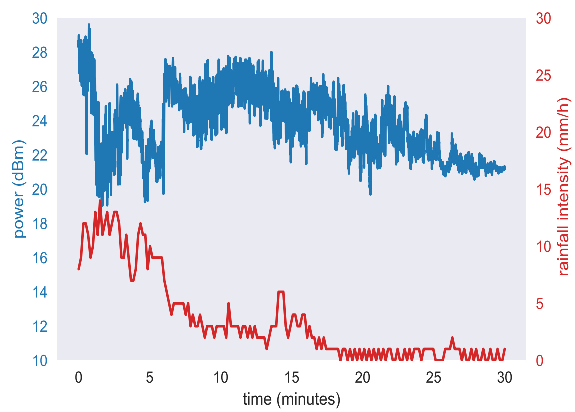

Figure 11: 23/12/2009,16:00-16:30

4.3 Drop Size Distribution

The main goal of this project is to investigate the possibility of retrieving an estimation of the drop size distribution (DSD) from the microwave link signals. Most work that has been done on using microwave links for precipitation measurements have looked at the attenuation of the signal, and from this, estimating path-averaged rainfall intensities. The difference in this study is that we propose to measure the drop size distribution. This distribution is important in many applications such as radar meteorology and cloud physics. Knowing the drop size distribution can also give us information on soil erosion. Interestingly, this is because the amount of soil that is lost during a rainfall event is a function of the kinetic energy of the precipitation, with larger drops having greater kinetic energy due to increased mass and terminal velocity. As we will show in this section a rainfall event will almost always have a range of different drop sizes, and so naturally the overall kinetic energy of any rain event will be dependent upon the drop size distribution. We will not focus too much on the use of the drop size distribution; however, in this section we will try to give the reader an idea of what the DSD is exactly, and how it is modelled in current literature.

Up until now we have assumed a mono-disperse distribution of raindrops, where we have used A to give us the number density, i.e. an approximation of the number of raindrops per unit volume. In real life situations it is not realistic to assume that all the raindrops are the same size, in actual fact the size of drops measured in rainfall usually range from about 0.3mm in radius up to about 5mm. When we are assuming a situation with a range of drop sizes we can label our new density function as $N(D)$. From here on, D will denote the diameter of a raindrop. We will use millimetres as units when describing this variable. It is important to note nonetheless that during any numerical computations involved in this study we have used metres. We start by giving a definition

Definition 4.1. *The drop size distribution is defined as the number of raindrops per unit volume per unit diameter.*

The units are $\mathrm{mm}^{-1}\mathrm{m}^{-3}$. This spectrum of drops is usually measured with an instrument called a disdrometer. This device works by measuring the vertical momentum of a raindrop falling onto its surface area, this momentum is then converted into a small electrical pulse. The amplitude of this pulse is then used to provide an estimate of the diameter of the raindrop that caused it. The disdrometer that we are using in this study measures the diameter of raindrops from 0.3mm up to 5mm, split up into 127 bins. From the data the volume distribution of drops can be calculated by the following well-defined formula

$$N(D_i)_t = \frac{n(D_i)_t}{A\Delta t v(d_i)\Delta D_i}, \tag{4.1}$$

where t represents the time interval over which the measurement was taken, $n(D_i)_t$ the raw drop count in the i^{th} bin, A the exposed surface area of the disdrometer's sensor, and ΔD_i is the interval between drop sizes. The terminal velocity of a raindrop is commonly predicted by the following formula

$$v(D_i) = 3.78 D_i^{0.67}. \tag{4.2}$$

The assumption that will be made here is that the drop size distribution is spatially homogeneous, and stationary over the interval which we are measuring, for example 1 minute. We will show some plots of DSDs from which we can make some observations.

Here we have combined every six bins into one to get a smoother curve. We have also only plotted up to a drop size radius of 1.75mm. Several observations can be made from the plots below. In general the distribution is right- skewed, i.e. there concentration of smaller drops is much larger than that of larger drops. It can also be noted that we observe predominantly unimodel plots. It is true that there are small peaks for larger drops in certain minutes but there is in general one maximum.

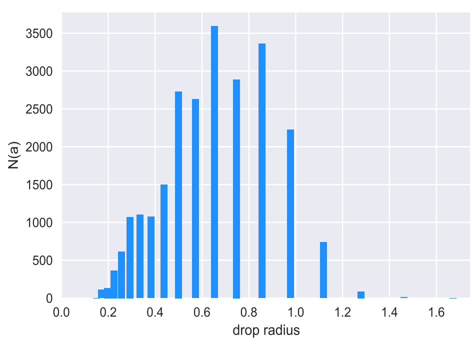

04:55am

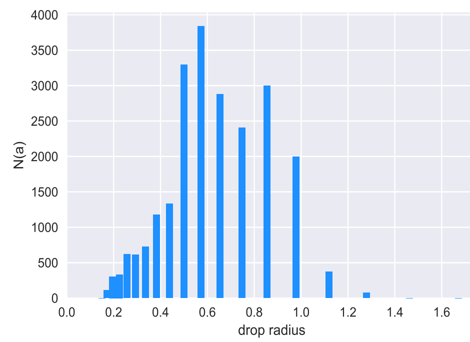

04:56am

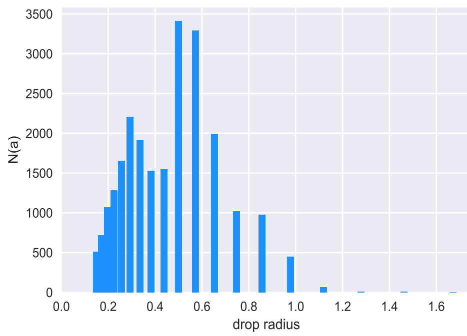

04:57am

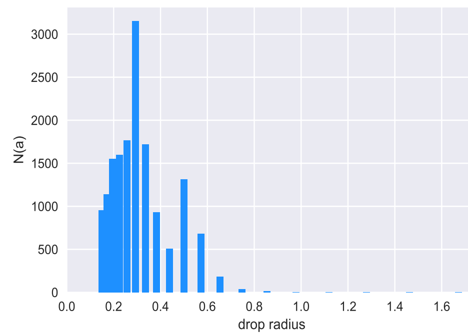

04:58am

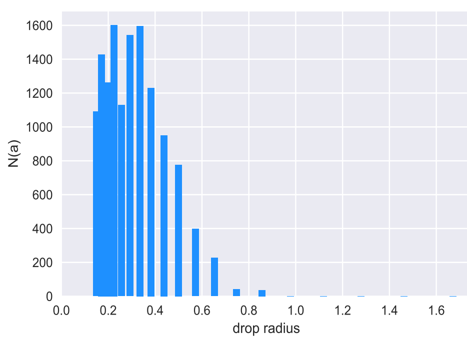

04:59am

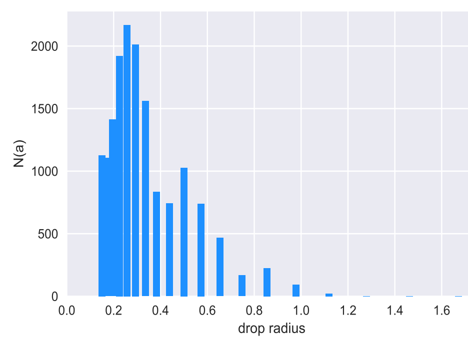

05:00am

In order to get more of an idea of the drop size distribution from a modelling perspective we first present one of the most known distributions that are used. The gamma distribution is written as

$$N(D) = N_0 D^w \exp(\Lambda D), \tag{4.3}$$

where Λ, w, and N_0 represent the slope, shape and scaling parameter respectively. It was found however, that for only a few samples this distribution tended to underestimate the number of drops which are in the range 0.3 to 1mm and overestimate those smaller than 0.3mm, which we show here.

From (4.1) we can consider defining the total number of drops $\forall D$ as

$$n(D_i)_t = n_t P(D_i)_t, \tag{4.4}$$

where n_t is the total drop count across all drops for some time t, D_i is the i^{th} drop, $P(D)_t$ is the probability distribution of raindrops, which we come to in the next section. Substituting the

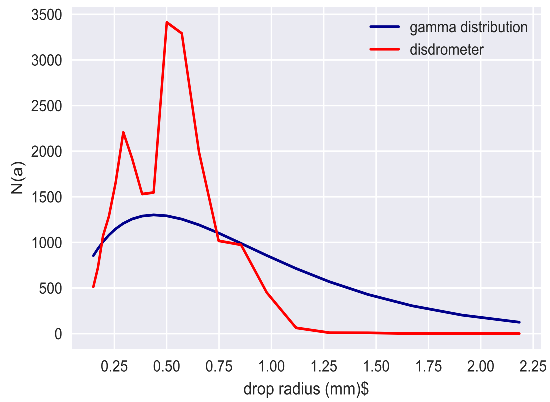

The Gamma Distribution plotted against disdrometer data, 04:57-04:58am, with a rainfall rate of 17 mm/h. Here N_0=8 $\times$ 10^{3}mm^{-1}m^{-3}, w=1 and λ=4.1$R^{-0.21}$ where R is the rainrate.

preceding equation into (4.1) gives

$$\begin{aligned} N_{D_i} &= \frac{n_t P(D_i)_t}{A\Delta t v(d_i)\Delta D_i} \\ &= \frac{N_t P(D_i)_t}{\Delta D_i}, \end{aligned} \tag{4.5}$$

where $N_t = \frac{n_t}{A\Delta t v(d_i)}$ represents the total drop count per unit volume.

These last comments provide an overall idea of the drop size distribution, which become more apparent in the inversion problem.

4.4 Comparison of the Spectrum

In order for it to be possible to compare theoretical predictions with real data we can no longer assume that we have a monodisperse distribution of raindrops. We need to incorporate the volume distribution of raindrops $N(a)$. We can rewrite (3.37) as

$$\mathcal{F}_D(f) = \int_{D_{min}}^{D_{max}} N(D)\mathcal{F}_\chi(f)dD. \tag{4.6}$$

where $\mathcal{F}_D(f)$ represents our forward model. Using thew Wiener-Khinchin theorem we can then say

$$\mathcal{P}_D(f) \approx \mathcal{F}_D(f) \tag{4.7}$$

where $\mathcal{P}_D(f)$ represents the power spectrum of the amplitude fluctuations, which is obtained directly from the data. We say approximately equal here because we haven't account for other phenomenon such as turbulence which can also cause amplitude fluctuations. We will now plot the temporal power spectrum of the amplitude fluctuations of the main signal along with our models prediction of the Fourier transform of the temporal covariance function. Here we plot the logarithmic frequency, and our time interval is one minute. As the rain rate can vary over a one minute period we have split each period into six intervals and taken an average. The rain rate is not included in (4.6), but we state the corresponding rain rate below obtained from data obtained from rain gauges. We illustrate the results below.

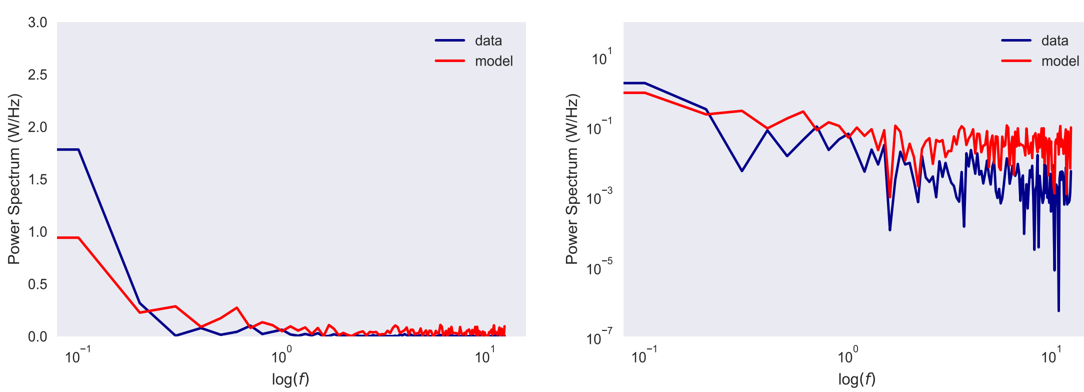

(a) Logarthmic x-axis

(b) Logarithmic x and y-axis

Figure 19: We plot the Power Spectrum of the data with the Fourier transform of the temporal covariance function. Here the data corresponds to that of 05:05am, with a rainrate of 1.2 mm/h.

From figures (19) and (20) we see that our theoretical output is an underestimation of the power spectrum for a lower rainfall intensity and for lower frequencies. This is most likely due to the effects of turbulence which we have not accounted for here. Turbulent eddies will have some

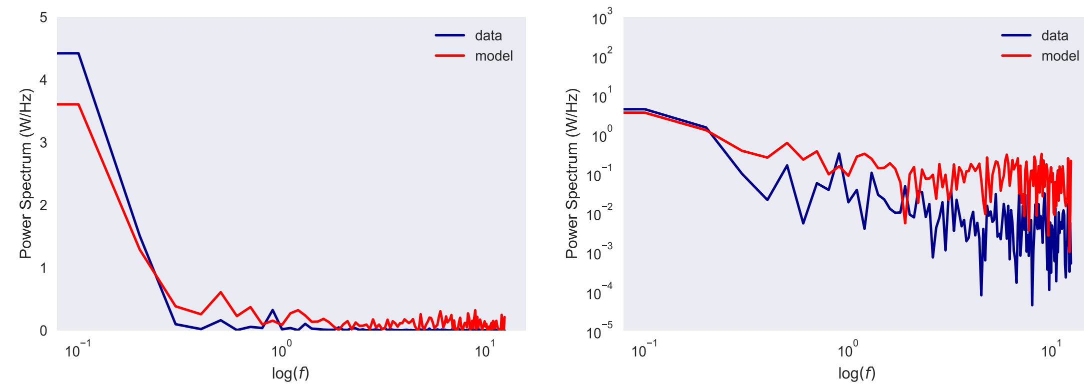

(a) Logarithmic x-axis

(b) Logarithmic x and y-axis

Figure 20: Here the data corresponds to that of 05:00am, with a rainrate of 3 mm/h.

effect on the overall signal, and particularly when we have a low rain rate, $\leq$3mm/h for example, the effects of turbulence become more apparent.

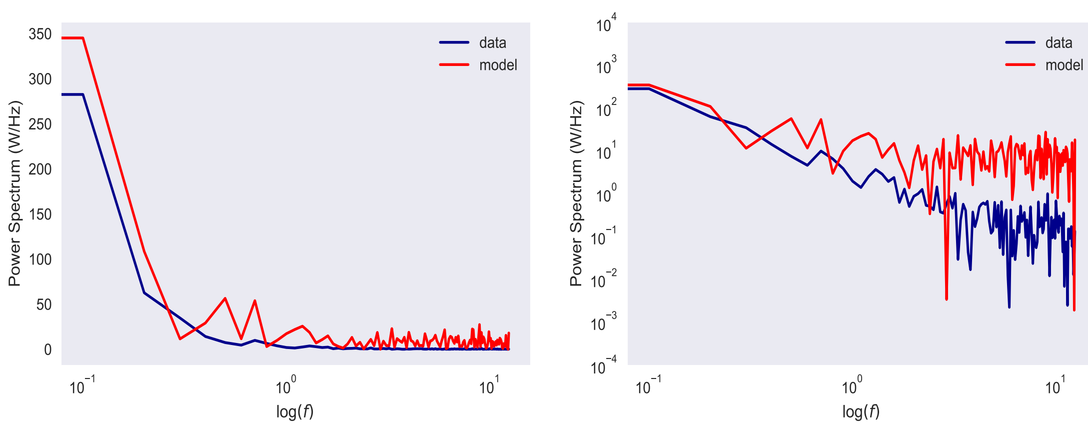

(a) Logarithmic x-axis

(b) Logarithmic x and y-axis

Figure 21: The data corresponds to that of 04:55am, with a rainrate of 38.7 mm/h.

When we have a much higher rain rate, like in figure (21) it is realistic to say that the amplitude fluctuations due to rainfall will be much more dominant than those from atmospheric irregularities. We also will not expect the data to show exactly what the model predicts. This is due to a number of factors, for instance we have not included the effects of multiple scattering, as the expressions would be far too complex. Moreover, we are considering a 500m path length and taking the drop size distribution to be constant throughout the spatial domain $0 < x < L$, whereas this will also most likely will not be the case. Lastly we have not taken into account any wind factor, which will most likely be present during heavy rainfall. This, along other atmospheric variables make it very difficult to obtain a model with an exact match to the data.

5 The Inversion Problem

5.1 The Theory

In the previous sections we have described our forward model which takes our derived Fourier transform of the amplitude fluctuations of a spherical electromagnetic wave and the known drop size distribution for some time t, to produce a theoretical prediction of the power spectrum of the signal.

We now take the drop size distribution as the unknown quantity of interest and use our model and the observed signal to make an inference on this. We denote our unknown quantity $\xi \in \mathbb{R}^n$, where n denotes the number of drop sizes, the signal from the microwave links we will denote d, and the known observation process we will denote H. In the absence of errors we have a forward map $H : \xi \to d$. Deterministic inversion problems make use of regularization to produce a point estimate of parameter ξ. Probabilistic methods present the most likely solution of the problem, from an average over all possible solutions. We can see from above that our solution is not exact, i.e there is noise present in the model. Naturally the noise is probabilistic and so the key point in our problem is that we want to quantify the uncertainty on any measurement noise present in the system and on our drop size distribution. This leads us to follow the Bayesian approach in order to gain as much information as possible on ξ. The advantage of statistical approaches is that they give more than just a single estimate, because the unknown quantity of interest is described as a probability distribution. These methods also take all prior information on the unknown parameters into account in a very systematic way, along with model and measurement errors. Moreover, inferential methods provide solutions where a large range of unknown parameters can be quantified.

To begin we can express our problem in linear form, where

$$d = H\xi + \epsilon,$$

where ϵ represents all noise present in the system, and is seen as a random variable. We can show this in matrix form as follows

$$\begin{bmatrix} \\ \\ d \in \mathbb{R}^f \\ \\ \\ \end{bmatrix} = \begin{bmatrix} & & \\ & & \\ & H \in \mathbb{R}^{f \times n} & \\ & & \\ & & \end{bmatrix} \begin{bmatrix} \\ \\ \xi \in \mathbb{R}^n \\ \\ \\ \end{bmatrix} + \begin{bmatrix} \\ \\ \epsilon \in \mathbb{R}^f \\ \\ \\ \end{bmatrix}$$

where H represents the Fourier transform of the amplitude fluctuations that we derived in section 2.

The probability of measuring the data d given that we have the real parameter set ξ is

$$P(d|\xi) = P(\epsilon = d - H(\xi)) = P_\epsilon(d - H(\xi)). \tag{5.1}$$

where P_ϵ represents the probability measure induced by the random variable ε. Arriving at a solution of the inverse problem involves drawing samples from $P(d|\xi)$, which we will show is a probability density function parameterised by ξ via the forward model H.

We explore what is known about the noise process and what we can say about it. Often only the statistical properties of noise ϵ are known. We will make the assumption that the noise in our system is additive white Gaussian noise. This additive noise is also taken to have zero mean as we are assuming there is no systematic error. We also assumed it is white, so that it has a constant power spectrum and hence there is no time correlation on the errors. Lastly, taking our noise to be Gaussian is a reasonable assumption by the central limit theorem. The theorem states that the distribution of the sum of a large number of independent random variables will tend towards a normal distribution, and so without knowing the error at each individual step in the process, we can assume the resultant error over the whole system will accumulate into a Gaussian distribution.

The key idea naturally in Bayesian Inference is to use Bayes rule to derive the posterior probability as a consequence of the prior probability and the likelihood function. This can be written as

$$P(\xi|d) = \frac{P(d|\xi)P(\xi)}{P(d)}, \tag{5.2}$$

where $P(\xi|d)$ represents the posterior distribution, $P(d|\xi)$ the likelihood function and $P(\xi)$ the prior probability.

Following from the fact that we have assumed the probability distribution of measurements errors to be normally distributed we define the likelihood function for observing the data d to be modelled by a multivariate Gaussian distribution which can be written as

$$P(d|\xi) \propto \exp\big(-\phi(d - H\xi)\big), \tag{5.3}$$

where $\phi(\cdot)$ represents the energy function of the system. Our assumption of noise being additive, white and normally distribution means the energy function takes the form $\phi(\cdot) = \frac{1}{2}(\cdot)\Sigma^{-1}(\cdot)$, so

$$P(d|\xi) \propto \frac{1}{(2\pi)^{n/2}|\Sigma|^{1/2}} \exp\big(-\frac{1}{2}(d - H\xi)^T\Sigma^{-1}(d - H\xi)\big), \tag{5.4}$$

where Σ represents the $n \times n$ covariance matrix and $|\Sigma|$ represents the determinant of Σ. Here n represents the number of unknown parameters, so the number of gradations we distribute our drop sizes into.

We have stated that the errors are identically and independently distributed random variables and so they are statistically uncorrelated, i.e. their covariance is zero, and so the covariance matrix of a white noise vector $\mathbb{R}^n$ will be an $n \times n$ matrix with the form $\Sigma = \sigma^2 I$. Here σ is the standard deviation of the measurement error and I represents the identity matrix.
We don't know the exact value for σ^2 and so we need to make an estimate. It should be noted that any electronic noise from the instruments used in the experiments can be treated as negligible compared with other sources of noise. We consider the most predominant source of noise to be the discrepancy between the forward model and the observed data. This is commonly known as the residual sum of squares, and defined as

$$RSS = \sum_{i=1}^{n} \hat{\epsilon}_i = \sum_{i=1}^{n} (d_i - H\hat{\xi}_i), \tag{5.5}$$

where $\hat{\xi}$ represents the predicted vector ξ. The problem we face is that because ξ is our vector of unknown parameters that we want to retrieve, we don't want the variance to be a function of the unknowns. We get around this by using a sample of data from the receiver, and corresponding disdrometer data. With a number of samples we can get an average value for our so called predicted outcome and use this to obtain an estimate of what the error will be. We do this by running our forward model, with known drop size distributions, along with the data for several rain events to work out an average difference between the two. We can then use this average as our measurement error, which can then be used in the inverse model for predicting the unknown parameters in the future. An estimation of the variance can then be written as

$$\hat{\sigma}_\epsilon^2 = \frac{1}{\hat{f} - n} \sum_{i=1}^{n} \hat{\epsilon}_i, \tag{5.6}$$

where $\hat{f}$ the number of frequency values we are considering. We use $\hat{f}$-n rather than $\hat{f}$-1 in the denominator to adjust for the estimation of the n-dimensional parameter ξ.

5.2 The Prior Probability

Now that we have some idea on how to model $P(d|\xi)$ we need to find a way to express our prior knowledge on our unknowns as a probability distribution. This step is crucial in Bayesian analysis and so a prior probability $P(\xi)$ must be chosen with care. In the case of Bayesian inference a prior gives us some idea of the probability of observing the true parameter value, before any evidence or data is taken into account. So instead of $P(D)$, as defined in (4.3) for example, we want $P(N(D))$, which we denote $P(\xi)$. In other words we don't want the probability of observing a drop, we want the probability of getting the correct volume distribution of each drop size.

It is also important to note that we are assuming to have no prior knowledge about the correlation between the different components of ξ. We can write this as

$$P(\boldsymbol{\xi}) = \prod_i P_i(\xi_i), \tag{5.7}$$

where i represents the number of different drop sizes. We have an abundance of data and so we can assume to have some knowledge about the expected value for each ξ_i. We also assume that the dispersion around the mean values is the same for each ξ_i. Under the assumption that our variables ξ_i are identically and independently distributed brings us to using a Gaussian prior law by the central limit theorem, which states that the probability distribution of the average of these random variables will approach a normal distribution. With this we have $\mathcal{N}(\mathbb{E}[\xi], \sigma_{\xi^2})$. This gives

$$\begin{aligned} P(\xi) &\propto \frac{1}{\sqrt{2\pi}\sigma_\xi} \exp\bigg(- \frac{1}{2\sigma_\xi} \sum_i |\xi - \mathbb{E}[\xi_i]|_{L_2}^2 \bigg) \\ &= \frac{1}{\sqrt{2\pi}\sigma_\xi} \exp\bigg(- \frac{1}{2\sigma_\xi} ||\xi - \mathbb{E}[\xi]||_{L_2}^2 \bigg), \end{aligned} \tag{5.8}$$

where $\mathbb{E}[\xi]$ represents the assumed vector of expected values. This mean can be approximated over a large number of samples from different rainfall events. Substituting (5.4) and (5.8) back into (5.2) we obtain

$$P(\xi|d) \propto \exp\bigg(- \frac{1}{2\sigma_\xi} ||\xi - \mathbb{E}[\xi]||_{L_2}^2 - \frac{1}{2\hat{\sigma}_\epsilon} ||d - H\xi||_{L_2}^2 \bigg). \tag{5.9}$$

5.3 Maximum a posteriori estimate

Going back to (5.2) we note that we have not yet considered the function $P(d)$. In general, this term is known as the marginalised likelihood and is just a normalising finite constant. We will show now why this can be ignored in our retrieval of the drop size distribution. We will approximate the posterior distribution by taking the delta function approximation

$$P(\xi|d) \simeq \delta(\xi - \hat{\xi}^{MAP}), \tag{5.10}$$

where $\hat{\xi}^{MAP}$ corresponds to the maximum a posterior estimate (MAP) and can be written as

$$\hat{\xi}^{MAP} = \arg\max_\xi P(\xi|d). \tag{5.11}$$

The maximum a posterior estimate returns the values which maximise the posterior distribution, i.e. the set of parameter values that make observing the true parameters given we observe the data the most likely. In other words the maximum a posteriori estimate gives us the mode of the posterior distribution. Substituting (5.2) into the above equation gives

$$\hat{\xi}^{MAP} = \arg\max_\xi \frac{P(d|\xi)P(\xi)}{P(d)} = \arg\max_\xi P(d|\xi)P(\xi), \tag{5.12}$$

because the denominator in this instance has no dependence on ξ and so will play no part in the optimisation.

Both our likelihood function and our prior distribution involve exponentiation. We can simplify these expressions by considering the logarithm of these functions. This is possible because taking the log is a monotonic transformation and a strictly increasing function, so will have a maximum at the same point, and so we can greatly simplify our expression but maintain the same optimal result. We can write the log-likelihood as

$$\begin{aligned}\log \mathcal{L}(\xi, d) &= \log \prod_i P(d|\xi_i)P(\xi_i) \\ &= \sum_i \log P(d|\xi_i)P(\xi_i)\end{aligned} \tag{5.13}$$

From (5.7) we are assuming a statistically independent set of parameters and so the MAP will be the product of individual estimates

$$\hat{\xi}^{MAP} = \arg\max_{\xi} P(d|\xi)P(\xi) = \arg\max_{\xi} \prod_i P(d|\xi_i)P(\xi_i). \tag{5.14}$$

Taking the logarithm, as seen from (5.13), results in the following

$$\hat{\xi}^{MAP} = \arg\max_{\xi} \sum_i \log(P(d|\xi_i)P(\xi_i)). \tag{5.15}$$

Substituting the prior and the likelihood function into (5.13) gives the log-likelihood as

$$\begin{aligned}\log \mathcal{L}(\xi, d) &= \log \left[\exp\left(-\frac{1}{2\sigma_{\xi_i}} ||\xi - \mathbb{E}[\xi]||^2_{L_2} - \frac{1}{2\hat{\sigma}_{\epsilon_i}} ||d - H\xi||^2_{L_2} \right) \right] \\ &= -\frac{1}{2} \left(\frac{1}{\hat{\sigma}_{\xi}} ||\xi - \mathbb{E}[\xi]||^2_{L_2} + \frac{1}{\hat{\sigma}_{\epsilon}} ||d - H\xi||^2_{L_2} \right).\end{aligned} \tag{5.16}$$

From a computational point of view we will minimise the negative of the log-likelihood to obtain the maximum a posterior estimate. We write this as

$$\hat{\xi}^{MAP} = \arg\min_{\xi} -\log \mathcal{L}(\xi, d). \tag{5.17}$$

5.4 Results

We will approximate (5.17) with a gradient-based algorithm, and test on signal data from 16^{rd} January 2010. We obtain various statistical properties, like the error variance from samples from October 2009, in periods where there was known to be rainfall. Once we had 'trained' the model on previous data we could use it to predict the drop size distribution for signals where the drop size distribution is unknown.

Although it is taken to be unknown we plot the disdrometer data next to the result of the Bayesian analysis result to compare how well the model worked.

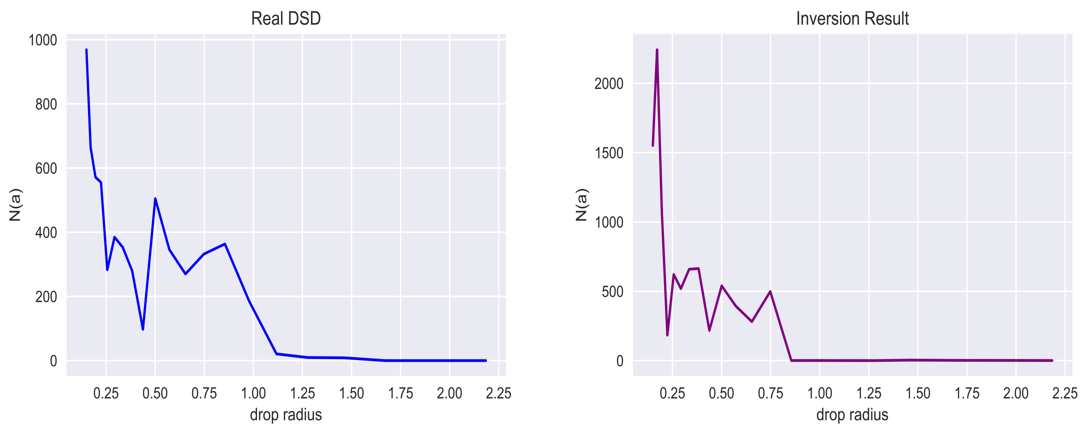

Figure 22: 16/01/2010,19:55-19:56

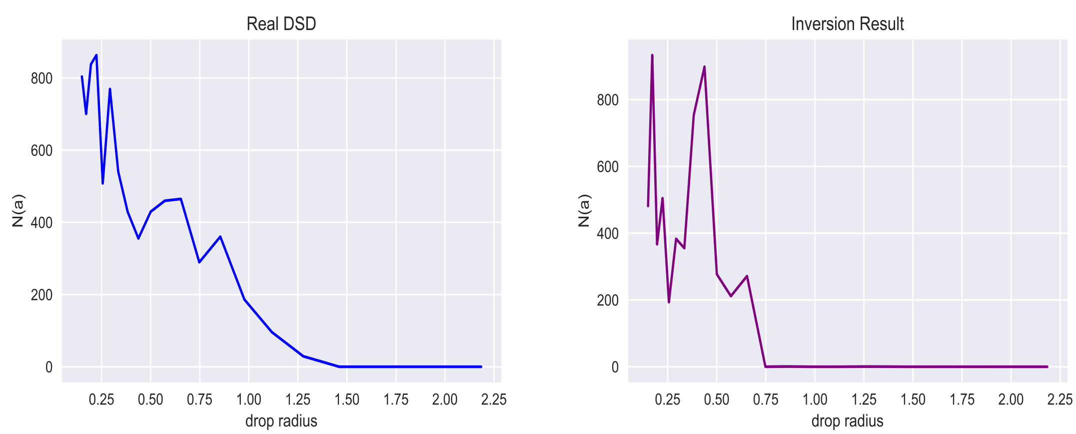

Figure 23: 16/01/2010,19:56-19:57

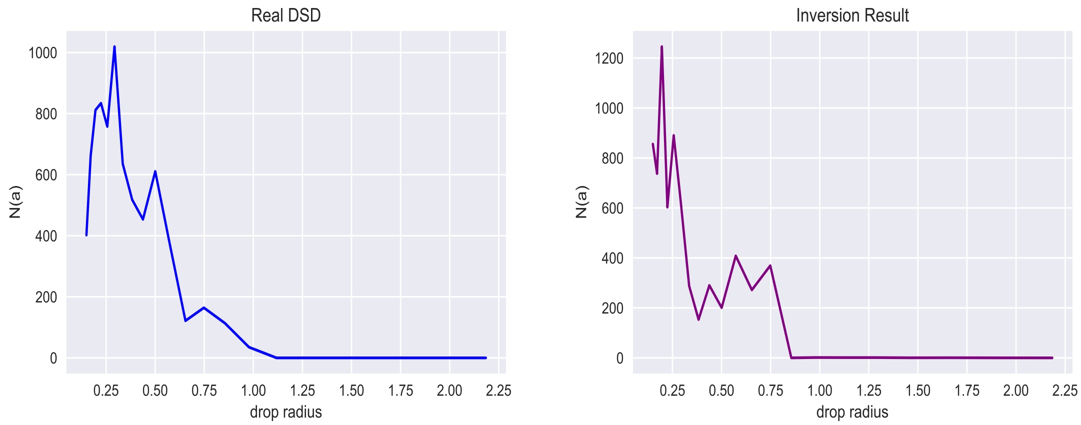

Figure 24: 16/01/2010,19:57-19:58

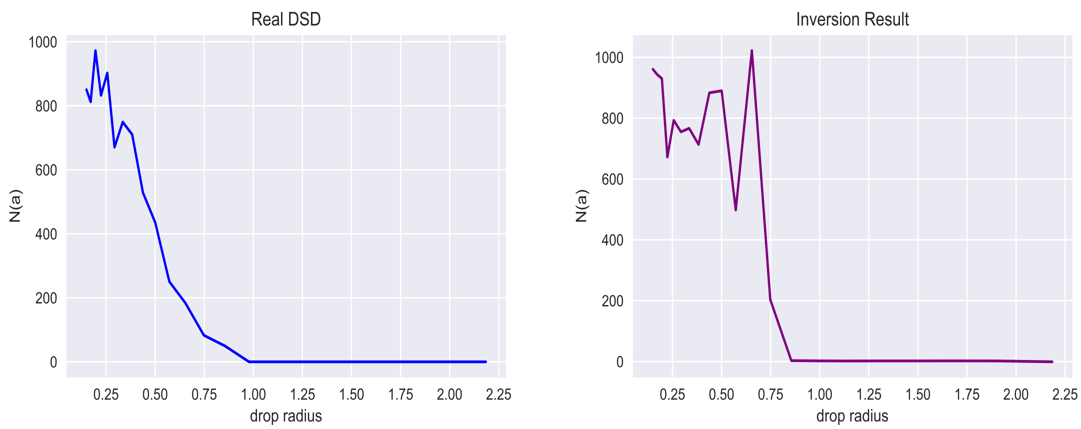

Figure 25: 16/01/2010,19:58-19:59

We plot the result for six different times. We again take an average over six ten second intervals over the stated minute. The disdrometer gradations were also combined into 21 bins, rather than the measured 127 to give a smoother curve. Another reason for this is so that we reduce the number of parameters to be estimated by a factor of 6, in the hope for faster convergence of the algorithm. Furthermore, the Fourier transform is a linear transform that takes signal from time domain to the frequency domain and hence the number of time points will be equal to the number of frequency points. If we want to consider a retrieval of the drop size distribution over 10 seconds, or one minute for example, we would not expect as good a result, if any, if we wanted to estimate 127 different parameters. It also makes sense to consider shorter time intervals, otherwise the values in the disdrometer data and in the Fourier transform of the signal will be of a higher order or magnitude, and so more room for error. Taking the Fourier transform over 10 minutes for example also won't give much information as the rain rate can fluctuate a huge amount in a short

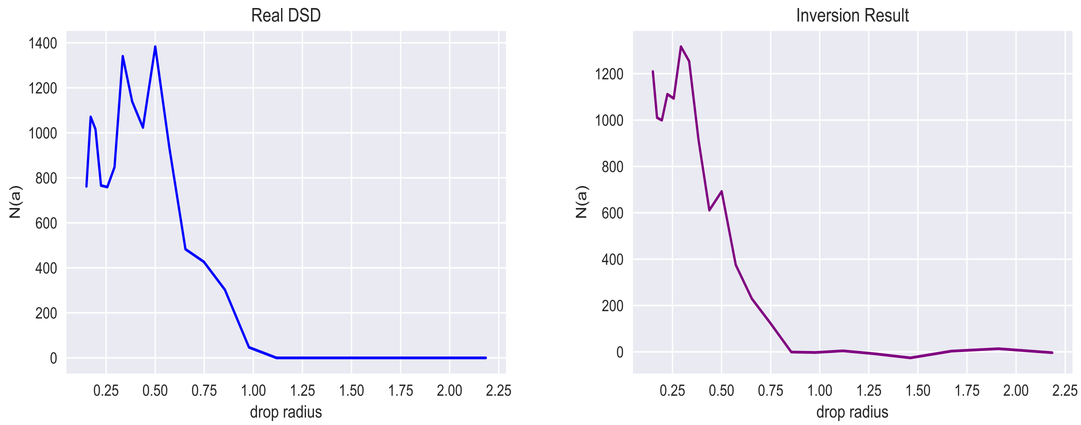

Figure 26: 16/01/2010,19:59-20:00

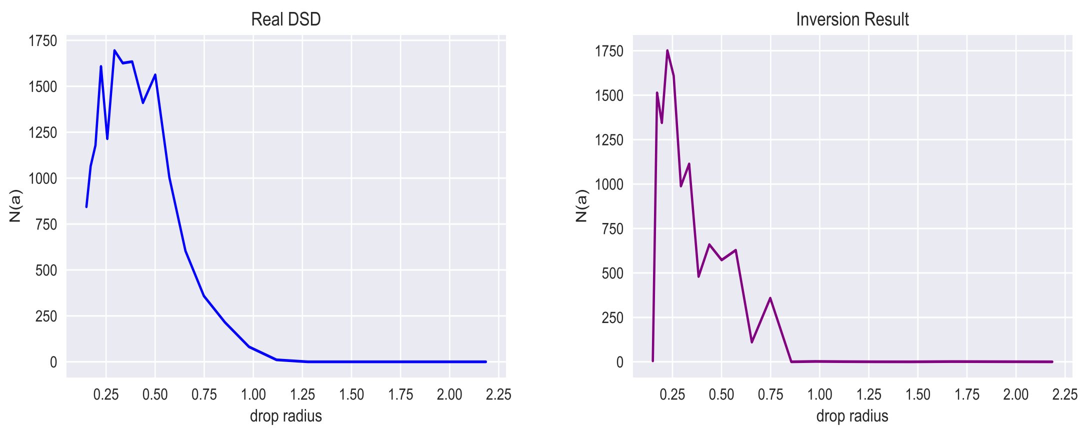

Figure 27: 16/01/2010,20:00-20:01

space of time. In addition, we're assuming the rain to be a statistically stationary process over the time interval that is considered. The validity of this assumption is likely to rapidly decrease with increasing time interval.

It is clear to see that the results shown in the above figure are not the exact drop size distribution; however, it is a promising start. Considering that there are many errors involved in the measurement process, not just from the model but also from the fluctuations of the signal itself, the outcome was uncertain, especially as this is the first known study of this method. The most promising aspect is that the shape and order of magnitude are reasonably correct. Perhaps with a more appropriate prior or using Markov Chain Monte Carlo Methods which sample from the whole posterior distribution rather than just the mode, might result in a better outcome.

We can go further in the comparison and see if the retrieved volume distribution of raindrops shows a similarity to the measured rain rate. This can be done by the following estimation (reference)

$$R_t = \frac{\pi}{6} \times 3.610^{-3} \int_0^\infty D^3 V(D) N(D) dD, \tag{5.18}$$

where R_t is the instantaneous rain rate in mm/h, and $D = 2a$.

Rainfall Rate			
Time	Rain Gauge	Real DSD	Inversion Result
19:55	3.1	2.7	2.5
19:56	5.0	4.3	3.7
19:57	1.8	1.2	0.8
19:58	1.4	1.2	1.5
19:59	2.7	2.6	2.3
20:00	2.5	2.1	1.8

In general the results from the table above show us that the results are promising. A possible reason for the difference in values between the rain gauge data and that measured using (5.17) are maybe to do with how much the rain rate can change over one minute. The inversion results show a slight underestimation for most cases of the rainfall intensity; however, in general the estimate is reasonable.

6 Conclusion, Discussion and Future Work

At the start of this thesis it was shown that it is possible to obtain an expression for the temporal amplitude covariance, using Mie's scattering theory as a starting point. We note that in general the key to these spectrum's showing a shape similar to that of the Power Spectrum of the data is the amplitude function $S(\theta)$, which must be a function of frequency. We initially made the assumption that $S(\theta) = S(0)$, i.e. that we are assuming forward scattering; however, even though the scattering angles can be taken to be extremely small, they must still vary with f, at least for the analysis. If we take S to be constant for each drop size, the trigonometric functions involved become dominant and we get a far more oscillatory function appearing.

Following on from this we defined prior and posterior probabilities to the drop size distribution and the power spectrum of the signal. Several prior possibilities were tried, like a gamma distribution for example; however, convergence was very slow. In general the Gaussian prior showed the most promising results. As an idea for future work, possibly the dispersions of the parameters from their mean value could be taken to follow a distribution rather than be assumed constant, to account for more likely variability in values for the smaller drop sizes.

One might also want to consider adding the effects of turbulence into the model. This has not been done here; however, Tatarskii [4] for example gives a rigorous anaylsis on the effects of atmospheric turbulence on electromagnetic wave propagation. This might help with explaining the differences observed between the forward model $\mathcal{F}_D(f)$, as defined in (4.6) and the power spectrum of the signal, particularly in the lower frequency regions for example.

Multiple scattering is also something one could consider. We have not included the effects of multiple scattering in our analysis because the raindrops are far enough apart that we can take single scattering to be the most dominant. However, in some types of precipitation, such a drizzle, where there are a very large number of small drops, this assumption might not be as valid. In heavier rainfall, where there are fewer but much larger drops, the assumption of single scattering is more valid. Moreover, multiple scattering consider second, third and so on order of functions, so how much effect this would have on our expressions for the amplitude fluctuations due to rainfall is unknown, but we expect the difference won't be substantial.

We also found that for certain time frames, the data produced far less smooth curves for the power spectrum than others. Definite spikes were present for high and low frequencies. It would be impossible to know the exact reason for this, but this resulted in a worse match to the disdrometer data in the retrieval. This was only for a small number of cases but perhaps if more time was available this could be looked into further.

We have shown that we can also obtain information about the rainfall intensity from the drop size distribution in (5.18). It is much harder to do this the other way around, and so estimating the drop size distribution directly could be an invaluable technique.

If we wanted to apply this method to using data from microwave links used in mobile phone networks, something worth noting is the difference in sample frequency. In the data we had access to for this study, the signal was sampled at 25Hz, whereas typically mobile phone network sample at frequencies much lower than this, so this would need to be taken into account when using the model.

Overall this method for the retrieval of the drop size distribution has great potential, particular because several atmospheric variables were not accounted for. This may partly be due to the fact that, as we can see from Figure 5, the spectrum for each individual drop size is quite different, and so this will help considerably in the inversion problem. There is more work to be done here; however, it is a definite start in using spectral analysis methods to obtain the drop size distribution from microwave link data.

References

[1] A. Overeem, H. Leijnse, and R. Uijlenhoet (2013) Country-wide rainfall maps from cellular communication networks *Proc. Nat. Acad. Sciences*, 110:2741–2745.

[2] Statista (2016) Number of mobile phone users worldwide from 2015 to 2020 (in billions). Available at https://www.statista.com/statistics/274774/forecast-of-mobile-phone-users-worldwide/.

[3] T. Wang (1975) Use of rainfall-induced optical scintillations to measure path averaged rain parameters.*Journal of the Optical Society of America*,1975,65,927-937.

[4] V.I.Tatarskii (1971) The effects of the turbulent atmosphere on wave propagation. Translated from Russian by Israel Program for Scientific Translation.

[5] Rayna Hollander (2017) Two-thirds of the world's population are now connected by mobile devices. Available at https://www.businessinsider.com/world-population-mobile-devices-2017-9?international=truer=USIR=T. (2 in thesis)

[6] H.C.van de Hulst (1957) Light scattering by small particles New York, Dover Publications, 1957.

[7] A. Wheelon (2001) Electromagnetic Scintillation I. Geometrical Optics, Cambridge University Press, Cambridge.

[8] A. Wheelon (2003) Electromagnetic Scintillation II. Weak Scattering, Cambridge University Press, Cambridge.

[9] Charles Zufferey (1972) A study of the rain effects of electromagnetic waves on electromagnetic waves in the 1-600 GHz range. Masters Thesis, University of Colorado Boulder.

[10] J.S.Marshall and W. McK. Palmer (1948) The distribution of raindrops with size. *Journal of Meteorology, 165-166*

[11] Kohei Arai (2016) Size Distribution Estimation Method using Reflected Laser Light Angle Dependency by Rain Droplets.*International Journal of Advanced Research in Artificial Intelligence, Vol. 5, No. 12,http://dx.doi.org/10.14569/IJARAI.2016.051201*

[12] K. C. Yeh (1962) Propagation of Spherical Waves Through an Iono- sphere Containing Anisotropic Irregularities, *Journal of research of the National Bureau of Standards, D. Radio Propagation Vol 66D, No.5, 621-636.*

[13] Bohumil Chytil (1969 Amplitude and phase scintillations of a spherical wave.*Journal of Atmosphearc and d Terrestrial physics,vol.32, 961-966*

[14] Ganjun Xu and Zhaohui Song (2016) A new model of amplitude fluctuations for radio propagation in solar corona during superior solar conjunction *Radio Science Article 10.1002/2015RS005769, AGU Publications.*

[15] Ganjun Xu and Zhaohui Song (2018) Amplitude fluctuations for optical waves propagation through non-Kolmogorov coronal solar wind turbulence channels. *Optics Express, Vol. 26, No. 7, AGU Publications, 8566-8580.*

[16] K'ufre-Mfon E. Ekerete, Francis H. Hunt, Judith L. Jeffery2, and Ifiok E. Otung (2015) Modeling rainfall drop size distribution in southern England using a Gaussian Mixture Model. *Radio Science Article 10.1002/2015RS005674, AGU Publications.*

[17] Ali Mohammad-Djafari (2001) Bayesian inference for inverse problems. *Laboratoire des Signaux et Systèmes.*

[18] D. Watzenig (2007) Bayesian inference for inverse problems– statistical inversion, *Elektrotechnik Informationstechnik, Springer-Verlag, Vol 8, 240-247.*

[19] D.Deirmendjian (1969) Electromagnetic Scattering on Spherical Polydispersions, *Report for United States Air Force Project Rand, Elsevier Publishing Company.*

[20] Fabrizio Frezza, Fabio Mangini and Nicole Tedeschi, (2017) Introduction to electromagnetic scattering: tutorial. *Vol. 35, No. 1 / January 2018 / Journal of the Optical Society of America A*

[21] Khaled M. Gharaibeh (2012) Nonlinear Distortion in Wireless Systems: Modeling and Simulation with MATLAB. *John Wiley Sons, Ltd. Published*

[22] K. Kalantar-zadeh (2013) Sensors: An Introductory Course, *Springer Science+Business Media New York.*

[23] Tamre P. Cardoso and Peter Guttorp (2008) A Hierarchical Bayes Model for combining Precipitation Measurements from Different Sources. *Progress in Probability, Vol. 60, 185–210*

[24] Guy Potvin (2015) General Rytov approximation. *Vol. 32, No. 10, Journal of the Optical Society of America A.*

[25] N. I. Fox. (2004) Technical note: The representation of rainfall drop-size distribution and kinetic energy. *Hydrology and Earth System Sciences Discussions, European Geosciences Union, 2004, 8 (5), 1001-1007*

[26] Leijnse, H., R. Uijlenhoet, and J. N. M. Stricker (2007), Rainfall measurement using radio links from cellular communication networks, *Water Resour. Res., 43*, W03201, doi:10.1029/2006WR005631.

[27] Mahadi Lawan Yakubu, Zulkifli Yusop, and Fadhilah Yusof (2014) The Modelled Raindrop Size Distribution of Skudai, Peninsular Malaysia, Using Exponential and Lognormal Distributions. *The Scientific World Journal* Volume 2014, Article ID 361703.

[28] J. M. D. Coey (2012) Signal and Noise [PowerPoint Presentation] Available at *https://www.tcd.ie/Physics/research/groups/magnetism/files/lectures/py5021 /MagneticSensors3.pdf*

[29] Al Nosedal (2015) Bayesian Inference for Simple Linear Regression [PowerPoint Presentation]. Available at *https://mcs.utm.utoronto.ca/ nosedal/sta313/stat313-bayes-regression.pdf*

[30] Simo Särkkä (2017) Bayesian Estimation of Parameters in State Space Models [PowerPoint Presentation] Available at *https://users.aalto.fi/ ssarkka/course*$_k$2016/*handout*8*.pdf*

[31] Gelman, A., Hill, J. (2006). Likelihood and Bayesian inference and computation. In Data Analysis Using Regression and Multilevel/Hierarchical Models (Analytical Methods for Social Research, 387-414). *Cambridge: Cambridge University Press.* doi:10.1017/CBO9780511790942.023

[32] Jonathan Balaban (2018) A Gentle Introduction to Maximum Likelihood Estimation, Available at *https://towardsdatascience.com/a-gentle-introduction-to-maximum-likelihood-estimation-9fbff27ea12f.*

[33] William Koehrsen (2018) Markov Chain Monte Carlo in Python A Complete Real-World Implementation. Available at *https://towardsdatascience.com/markov-chain-monte-carlo-in-python-44f7e609be98.*

[34] William Koehrsen (2018) Bayesian Linear Regression in Python: Using Machine Learning to Predict Student Grades Part 2. Available at *https://towardsdatascience.com/bayesian-linear-regression-in-python-using-machine-learning-to-predict-student-grades-part-2-b72059a8ac7e.*

[35] Alan Oppenheim and George Verghese (2010) Introduction to Communication, Control, and Signal Processing. *Massachusetts Institute of Technology.*